molecular pharmaceutics

pubs.acs.org/molecularpharmaceutics

Article

Microemulsion for Prolonged Release of Fenretinide in the Mammary Tissue and Prevention of Breast Cancer Development

Giovanna Cassone Salata, Isabella D. Malagó, Vanessa F. M. Carvalho Dartora, Ana Flávia Marçal Pessoa, Márcia Carvalho de Abreu Fantini, Soraia K. P. Costa, João Agostinho Machado-Neto, and Luciana B. Lopes*

Cite This: *Mol. Pharmaceutics* 2021, 18, 3401−3417

Read Online

ACCESS | Metrics & More | Article Recommendations | Supporting Information

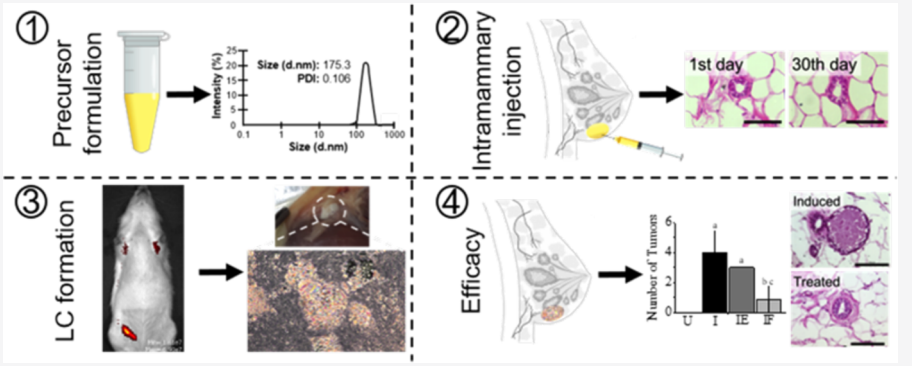

ABSTRACT: The need of pharmacological strategies to preclude breast cancer development motivated us to develop a non-aqueous microemulsion (ME) capable of forming a depot after administration in the mammary tissue and uptake of interstitial fluids for prolonged release of the retinoid fenretinide. The selected ME was composed of phosphatidylcholine/tricaprylin/propylene glycol (45:5:50, w/w/w) and presented a droplet diameter of 175.3 ± 8.9 nm. Upon water uptake, the ME transformed successively into a lamellar phase, gel, and a lamellar phase-containing emulsion *in vitro* as the water content increased and released 30% of fenretinide *in vitro* after 9 days. Consistent with the slow release, the ME formed a depot in cell cultures and increased fenretinide IC_{50} values by 68.3- and 13.2-fold in MCF-7 and T-47D cells compared to a solution, respectively. At non-cytotoxic concentrations, the ME reduced T-47D cell migration by 75.9% and spheroid growth, resulting in ∼30% smaller structures. The depot formed *in vivo* prolonged a fluorochrome release for 30 days without producing any sings of local irritation. In a preclinical model of chemically induced carcinogenesis, ME administration every 3 weeks for 3 months significantly reduced (4.7-fold) the incidence of breast tumors and increased type II collagen expression, which might contribute to limit spreading. These promising results support the potential ME applicability as a preventive therapy of breast cancer.

KEYWORDS: *microemulsion, in situ gelling, fenretinide, breast cancer, chemoprevention, sustained release.*

1. INTRODUCTION

Breast cancer is the most common type of neoplasm in women worldwide, second only to non-melanoma skin cancer, representing approximately 25% of all cancer cases.[1,2] Current strategies for prevention include mammographic screening (including mammography and breast ultrasound), preventive mastectomy, and oral chemotherapy with selective estrogen receptor (ER) modulators or aromatase inhibitors.[3−5] Apart from the mammographic screening, the other prevention strategies are not well accepted. Mastectomy causes important psychological impact and pain, while adherence to oral chemotherapy, represented by tamoxifen, raloxifene, and anastrozole, is low even in women at high risk of developing the disease, mainly due to the systemic adverse effects associated with these drugs.[3,6−9] Considering the high incidence of the disease, there is an overdue need for new, safer, and acceptable pharmacological strategies for prevention of breast cancer in high-risk population.

Motivated by this challenge, a delivery system capable of prolonging the release of the retinoid fenretinide within the breast tissue was developed in this study. Fenretinide (4-HPR) is a synthetic retinoid, derived from vitamin A, and displays apoptotic activity by multiple pathways, including caspase-3

Received: April 20, 2021
Revised: July 27, 2021
Accepted: July 28, 2021
Published: August 17, 2021

activation; suppression of the expression of NF-κB; elevation of reactive oxygen species levels; and, like other retinoids, regulation of the expression of proteins that mediate cell proliferation, differentiation, and apoptosis, due to its binding to retinoid receptors (RAR and RXR).[10−14] The drug has been considered a promising candidate for breast cancer prevention due to its improved safety profile compared to other retinoids and preferential accumulation in the mammary tissue.[15,16] To the best of our knowledge, the first report on the breast accumulation of fenretinide dates from the 1970s: fenretinide and its metabolite *N*-(4-methoxyphenyl)retinamide (4-MPR) were found in the breast tissue of rats fed with fenretinide for 6 months, while accumulation in the liver and its associated toxicity were not evident.[17] In a limited clinical study, Mehta *et al.* reported fenretinide and 4-MPR preferential accumulation in the breast tissue of patients,[18] which was corroborated by a subsequent study demonstrating 5-fold greater fenretinide concentrations in the breast tissue than in plasma when administered at 200 mg/day.[19] Consistent with these data, the nipple discharge concentration of fenretinide was approximately 13 times higher compared to plasma levels.[20]

Despite these pieces of evidence, there are no mechanistic studies that justify drug preferential accumulation in the breast tissue. Fenretinide is very lipophilic (log P = 6.31) and has a long terminal half-life of 13 h.[21] It has been reported to bind with high affinity to several proteins (including kinases) and tissues (including the buccal and subcutaneous tissue), and its non-specific binding has been related to interactions with cell membrane phospholipids.[22] Its accumulation in the mammary tissue might be attributed to its solubility in the fat compartment of the tissue, which constitutes a large portion of the breast.[19] The modification in the polar terminal group of the parent retinoid to produce fenretinide has also been suggested to impact the molecule *in vivo* distribution and breast accumulation.[17]

Fenretinide has been described to be cytotoxic against ER-positive and ER-negative breast cancer cells. The lack of preventive strategies for ER-negative tumors highlights one more advantage of this drug. This cytotoxicity supports the drug ability to destroy pre-existing tumor cells[13] while preventing the further development of lesions, enabling a "preventive therapy". In fact, fenretinide effectiveness for chemoprevention has been demonstrated in phase III clinical trials.[15,23]

However, fenretinide high lipophilicity, low oral bioavailability, and the consequent need for high daily doses (that increase the risk of adverse effects) make its incorporation in pharmaceutically acceptable formulations very challenging and hinder its clinical application.[15,24,25] To overcome these limitations while exploring fenretinide potential for breast cancer preventive therapy, we developed a non-aqueous microemulsion (ME) capable of undergoing phase transformation and gelling upon mammary administration and uptake of local fluids to provide prolonged fenretinide release in the breasts. To the best of our knowledge, delivery systems capable of increasing fenretinide concentrations in the mammary tissue in a prolonged manner as a preventive strategy for breast cancer have not been proposed. This study aims at filling this gap.

We acknowledge that part of the drug may be absorbed into the circulation, as observed after intramuscular administration of fenretinide suspension and PLGA microparticles (which produced systemic drug levels beyond 2 weeks)[26] as well as subcutaneous administration of fenretinide implants,[27] but by administering the drug in close proximity to the mammary tissue, we aim at taking advantage of its preferential accumulation at the site where it is supposed to exert its effects. The strategy proposed here finds support in previous evidence. First, as mentioned, fenretinide has high lipophilicity and tissue binding properties.[22] Second, previous studies demonstrated that topical drug administration to the breast skin (thus, in close proximity to the mammary tissue) resulted in similar breast distribution compared to oral administration but lower plasma levels.[28] Finally, subcutaneous administration of fenretinide-loaded PLGA implants placed alongside of oral squamous cell carcinoma tumors inhibited tumor xenographs with local controlled release, supporting the applicability of local fenretinide administration for chemoprevention.[27]

In this study, a phosphatidylcholine (PC)-based non-aqueous ME was developed as a precursor formulation for injection. The reasons for this selection are three-fold: first, PC is considered a biocompatible phospholipid capable of forming liquid crystals of the lamellar type upon contact with water, described to provide slower drug release compared to solutions but not as slow as the hexagonal or cubic phases.[29−31] The lower viscosity of this phase compared to other liquid crystals and implants has been associated with less discomfort to the patient.[32] Second, replacing water with propylene glycol (PG) and obtaining a non-aqueous ME improve fenretinide (a very lipophilic compound) solubilization.[33] MEs, generally described as isotropic dispersions of two non-miscible liquids in combination with a surfactant blend, have other advantages, including low cost, thermodynamic stability, and easy obtainment.[34,35] Third, due to the low viscosity, parenteral administration of MEs is less problematic compared to gels.[36]

In the first part of this study, the characteristics and phase behavior of the precursor ME, *in vitro* swelling kinetics, spreadability, and fenretinide release were characterized. In the second part, the *in vitro* effects of the fenretinide-loaded ME on breast cancer cell viability, migration, and proliferation were studied. The *in vivo* transformation, local irritation, and ability to sustain the release of a fluorophore were subsequently evaluated, and as proof of concept, the formulation efficacy at reducing breast cancer incidence was demonstrated using a preclinical model of chemical carcinogenesis.

2. MATERIALS AND METHODS

2.1. Materials. Tricaprylin was kindly supplied from Abitec Corporation (Janesville, WI, USA). Soy PC was obtained from Avanti Polar Lipids (95%, Alabaster, AL, USA), and PG was purchased from Synth (São Paulo, SP, Brazil). Fenretinide was obtained from Cayman Chemical (Ann Harbor, MI, USA). Evan's blue, phosphate-buffered saline (PBS), dimethyl sulfoxide (DMSO), tetrazolium dye 3-(4,5-dimethylthiazol-2-yl)-2,5-diphenyltetrazolium bromide (MTT), and 4′-6-diamidino-2-phenylindol (DAPI) were purchased from Sigma (St Louis, MO, USA). Other specific reagents (such as the ones employed in cell culture) are described along with the respective methodology. Ultrapure water was employed unless stated in the methodology employed at specific sections.

2.2. Non-aqueous ME Development and Phase Behavior in the Presence of Water. Non-aqueous MEs were obtained using tricaprylin (T) as the oil phase, propylene glycol (PG) as the polar phase, and PC as the surfactant. PG was selected as the polar phase because it modulates viscosity and is miscible with water, which enables phase transformation

https://doi.org/10.1021/acs.molpharmaceut.1c00319
Mol. Pharmaceutics 2021, 18, 3401−3417

upon uptake of aqueous body fluids. They were macroscopically characterized as single phase, transparent, isotropic, and fluid formulations.[33,37] The selection of tricaprylin was based on its ability to dissolve lipophilic drugs like fenretinide and the acceptable safety profile.[31] In addition to its ability to form liquid-crystalline phases, PC was selected due to its biocompatibility, which implicates in low irritation potential.[31,38]

PC and tricaprylin (T) (9:1, w/w) were vortex-mixed (Genie 2, Scientific Industries, Bohemia, NY) and heated at 50 °C in a water bath. Subsequently, PG was added to the PCT mixture at 40 and 50%, forming two MEs: ME 9:1−40% and ME 9:1−50% were composed of PC/T/PG at 54:6:40 and 45:5:50 (w/w/w), respectively. Subsequently, water was added at 1−80% to assess its influence on the phase behavior of the MEs and the formation of gels. The resulting formulations were visually inspected for transparency, phase separation, and fluidity, and visualized under a polarized light microscope (Carl Zeiss, Oberkochen, Germany).

2.3. Formulation Selection and Characterization. *2.3.1. Droplet Size of the Precursor Formulation.* Based on the viscosity and phase behavior, the ME composed of PC/T/PG at 45:5:50 (w/w) was selected for further characterization. Size and polydispersity index (PDI) were determined by using Zetasizer NanoZS90 equipment (Malvern, UK) after diluting the ME in PG (1:100 v/v)[33] to avoid phase transition.

2.3.2. Influence of Water on the Internal Structure and Rheological Behavior of the Formulations. To confirm the results from polarized light microscopy concerning phase behavior and predict characteristics of the systems that might be formed *in vivo* upon contact with interstitial fluids, the MEs prior and after addition of water at various contents were analyzed using small-angle X-ray scattering (SAXS) and a rheometer.

For SAXS analysis, water was added at 5, 10, 30, 50, and 80%, and after equilibration for 1 day, samples were analyzed using a Bruker AXS Nanostar SAXS camera with a microfocus Genix 3D system (source of copper Kα radiation, λ = 0.15418 nm plus focusing mirrors), two scatterless slit sets for collimation, and a 2D Vantec-2000 detector. The systems were placed in glass capillary sample holders. The acquisition time of each scattering curve was 15 min at room temperature. The intensity measurements were performed as a function of the scattering vector q ($q = 4\pi \sin\theta/\lambda$, where θ is half of the scattering angle). The sample−detector distance was 667 mm, which provided a q-range of 0.01−0.35 Å^{-1}. The scattering from the sample holder was subtracted from the scattering of each sample, the results were corrected by the detector response, and the SAXS data were normalized to take into account the transmission for each case.

The rheological behavior of the selected ME and its counterparts formed after addition of water at final concentrations of 20 and 80% was investigated using an R/S Plus controlled stress rheometer with the RC75-1 geometry (Brookfield Engineering Laboratories, Middleboro, MA) and a water bath circulator for temperature control (25 °C). The experiments were performed with shear rates varying up to 500 s^{-1}.

2.4. Evaluation of the *In Vitro* Swelling Rate and Spreading of the Formulation. The experiments described in this section had three main objectives: to assess the rate of uptake of aqueous fluids, how fast the liquid-crystalline phase would be formed upon contact with these fluids, and if the selected ME would spread on the tissue immediately after administration or would be contained due to its fast transformation in the semi-solid system.[36,39]

To study phase transition due to water uptake, precursor MEs were placed in cell culture inserts (Cell Culture Insert 353103—Falcon, USA, 1.0 μm pores) in contact with 3% alginate gel and incubated at 37 °C (to mimic the biological temperature). The use of a gel instead of water solutions was based on its ability to better mimic the subcutaneous and mammary tissues since water in tissues does not act like bulk water (it is not freely available) but is mostly associated with cell components.[40,41] Aliquots of the formulations in the inserts were collected and visualized at 2−24 h under a polarized light microscope to assess when the lamellar phase would be formed.[39] To monitor the rate of water absorption and determine the swelling kinetics, a parallel set of experiments was conducted, in which the cell culture inserts containing the formulation and placed in contact with a 3% alginate gel at 37 °C were weighed at regular intervals between 3 and 48 h.[39] A cellulose dialysis membrane (MW cutoff 1000 Da) was placed between the gel and the cell insert to prevent adhesion of the gel on the inserts (which would hinder the accurate insert weighing). The results of the amount of water absorbed as a function of time were expressed graphically. The data were analyzed using first-order $[\ln W_\infty/(W_\infty - W) = kt]$ or second-order $[t/W = 1/(kW_\infty^2) + t/W_\infty]$ kinetic equations, where W_∞ is the maximum amount of water absorbed by the formulation as a function of time (t), $W_\infty - W$ is the amount of water not absorbed, and k is the proportionality constant.[42]

To anticipate how much it could spread in the tissue after administration, the selected ME (100 μL) was stained with Evan's blue dye to facilitate visualization and placed on the top of a layer of sodium alginate gel (3%, 3 mL).[43] The area that the formulation occupied on top of the gel was measured from 30 s to 21 h (ImageJ software, USA) and compared to a PG control solution of the dye, which did not have the ability to transform into gels but whose viscosity was closer to that of the selected ME.

2.5. Short-Term Physical−Chemical Stability and Fenretinide Incorporation and Release. Fenretinide was dissolved in the oil phase of the selected ME by vortex mixing to obtain final concentrations varying between 1 and 5% (w/w). The formulations were analyzed macroscopically and under polarized light microscopy to identify the presence of drug crystals dispersed/suspended in the formulation. Subsequently, water was added at 1−80% (w/w), and the resulting formulations were visualized under polarized light microscopy to assess the influence of drug concentration on phase transition.

To assess fenretinide release, the formulations were placed in small dialysis bags (a 14,000 Da cutoff, Sigma-Aldrich, St. Louis, MO, USA) and placed in the receiver compartment of Franz diffusion cells (PBS buffer, pH 7.4, 1% polysorbate 80, 7 mL) maintained at 37 °C under stirring (200 rpm). The volume of receptor phase displaced when the dialysis bag was introduced in the receptor compartment of the diffusion cell was assessed by measuring the weight of the diffusion cell with and without the dialysis bag. Polysorbate 80 (1%) was included in the receptor phase to increase drug solubility (to approximately 500 μg/mL). For comparison with ME and to assess whether the membrane limited drug diffusion, a drug solution in PG was used as a control. Aliquots of the receptor phase were withdrawn (0.2 mL) at predetermined times (2 h

https://doi.org/10.1021/acs.molpharmaceut.1c00319
Mol. Pharmaceutics 2021, 18, 3401−3417

to 9 days) for drug quantification by spectrophotometric analysis at 365 nm (SpectraMax Plus 384, Molecular Devices).[44] The method was linear in the range of 5−100 μg/mL. To ensure the absence of interference of formulation compounds on the analytical method, unloaded MEs (without fenretinide) were placed in the dialysis bags, and the receptor phase was assayed at 365 nm at 24 h and 9 days. No interference was observed.

To assess the release kinetics, the amount of drug released was represented following the zero-order kinetics, represented by the equation $Q_t = Q_0 + K_0 t$; Higuchi kinetics, represented by $Q = K_h t^{1/2}$; and first-order kinetics, represented by $\log Q_t = -\frac{K_t}{2303} + \log Q_0$, in which Q_t represents the absolute amount of drug released in t (time in hours), Q_0 is the initial amount of drug in the solution, K_0 is a zero-order kinetic constant, and K_h is the Higuchi dissolution constant.[45]

A short-term, preliminary assay to assess the physical−chemical stability of the ME for 30 and 60 days was performed. Unloaded and fenretinide-loaded MEs (two batches each) were maintained at room temperature (25 °C maintained by air conditioning) in conical tubes protected from light. Subsequently, they were macroscopically assessed for phase separation and microscopically analyzed for the presence of drug crystals or changes in the ME isotropy. No macroscopic alterations, presence of drug crystals, and changes on the isotropy were observed during the studied period, suggesting that the main characteristics of the formulation were maintained in the presence of fenretinide.

2.6. Cellular Effects of the Formulation. To assess whether and how the incorporation of fenretinide in the formulation affected cell viability, migration, and proliferation, 2D cultures of MCF-7 and T-47D obtained from ATCC (Manassas, VA, USA), were maintained at 37 °C in a humid atmosphere with 5% CO_2 in 25 cm^2 flasks with the Dulbecco's modified Eagle's medium (DMEM) GlutaMAX culture medium supplemented with 10% fetal bovine serum (FBS) (Gibco/Invitrogen, USA), 50 μg/mL penicillin, 50 μg/mL streptomycin, and 0.5 μg/mL amphotericin B. These cell lines were selected because MCF-7 and T-47D are hormone-dependent (ER+) lines widely used as models for *in vitro* studies as they mimic between 79 and 84% of breast cancer cases worldwide.[46] Furthermore, one of the fenretinide proposed mechanisms to induce apoptosis is through caspase-3;[13] these two cell lines differ in caspase-3 expression (MCF-7 cells lack the protein while T-47D express it),[47] hence enabling us to assess the influence of this characteristic on the formulation cytotoxic and antimigratory effects.

2.6.1. Effects of the Formulation on Cell Viability. Upon reaching approximately 80% confluence, the cells were treated with trypsin (0.25%, Gibco/Invitrogen, USA) and transferred to 96-well plates at a density of 5000 cells/well. The cells were subsequently treated with the selected unloaded ME (2.5−100 mg/mL), ME containing fenretinide (ME-F, 2.5−100 mg/mL, fenretinide at 63.9−2557.5 μM), or the drug solution (0.01−255.40 μM) for 72 h. Since our goal was to mimic the *in vivo* scenario, predetermined amounts of the ME were carefully added dropwise close to the border of the well to enable the formation of a depot and avoid mixing with the culture medium. Supporting Information Figure S1 depicts an image of the setup when the highest ME amount employed was added to the well. This is a relevant difference from the experimental setup employed in previous studies in which MEs were mixed with the cell culture medium prior to treatment.[37,48]

At the end of the treatment, the medium was aspirated and the cells were incubated at 37 °C in the medium containing 0.5 mg/mL MTT. After 3 h, the medium was replaced with DMSO, followed by determination of absorbance at 595 nm in a Multiskan FC Microplate Photometer 51119000 plate reader, from Thermo Fisher Scientific (Waltham, MA, USA).

The values of the concentration necessary to reduce cell viability to 85% (or reduce viability by 15%, referred to as IC_{15}), 70% (or reduce viability by 30%, referred to as IC_{30}), 50% (or reduce viability by 50%, referred to as IC_{50}), and 30% (or reduce viability by 70%, referred to as IC_{70}) were determined and guided the formulation concentrations employed in subsequent experiments.

2.6.2. Effects of the Formulation on Cell Migration. The formulation effects on cell migration were investigated using T-47D cells placed in migration inserts (a density of 1×10^4 cells, Nunc, Thermo Fischer Scientific, Waltham, MA, USA) containing 300 μL of FBS-free DMEM GlutaMAX. In each well of the 24-well culture plates, 600 μL of the medium with 10% FBS was added for the chemoattractive role.[49]

On the day of the experiment, each insert was either untreated (maintained with the FBS-free medium) or treated (as described above) for 24 h with the unloaded ME or ME containing fenretinide (1%, ME-F) at the concentration equivalent to IC_{15} for 24 h. After treatment, the migration inserts were collected, and cells that were unable to migrate through pores and remained in the upper part of the membrane were gently removed with cotton swab.[49] Cells that migrated through the pores were fixed for 10 min in cold methanol 100% and stained in a dark environment with Fluoroshield solution with DAPI. Using a fluorescence microscope, all the quadrants of each insert containing the cells were photographed. The images were then analyzed in the ImageJ (National Institutes of Health, Bethesda, Maryland, USA) software for cell counting.

2.6.3. Effects of the Formulation on Cell Proliferation. The effect of the selected ME (at non-cytotoxic concentrations) on cell proliferation was assessed by measurement of the Ki-67 proliferation pathway on T-47D cells using flow cytometry and the anti-Ki-67 FITC marker (BD Bioscience, San Jose, CA, USA).[50] The cells were plated at 1×10^6 cells per Petri dish (60 × 15 mm) and treated for 48 h with the unloaded or fenretinide-loaded ME at IC_{15}. Treatment with ME at IC_{70} was employed as an additional control to ensure that a reduction in Ki-67 could be observed at cytotoxic concentrations. After treatment with trypsin, cells were fixed with 70% ethanol and stored at −20 °C for 24 h. Then, the staining protocol was performed following the standardized protocol by the manufacturer, and subsequent analysis on the FACScalibur Flow Cytometer (BD Biosciences) was conducted.

2.7. Assessment of Formulation Efficacy in 3D Models. To better mimic the morphological and functional characteristics of *in vivo* tissues, T-47D spheroids were employed as a 3D model of breast cancer. Spheroids were produced using the liquid overlay technique,[51] which does not allow cell adhesion to the plate surface. Thereunto, 96-well microplates were prepared by the application of 50 μL of 1% agarose solution to each well prior to the addition of T-47D cells (5 × 103 cells/well). After centrifuging (262.4×g, 7 min), the plates were incubated at 37 °C in a 5% CO_2 atmosphere.

https://doi.org/10.1021/acs.molpharmaceut.1c00319
Mol. Pharmaceutics 2021, 18, 3401−3417

Two assays were conducted. To evaluate the formulation effects on spheroid viability, one set of plates was treated with the loaded ME at IC_{15} and IC_{50} for 24 h after centrifugation. As a control of the effects of the unloaded formulation, cells were treated with ME (without fenretinide) at IC_{50}; since no significant reductions on spheroid viability were observed, the smaller concentration of the unloaded ME was not assessed. Treatment was maintained for 4 days, and viability was assessed using the CellTiterGlo 3D kit, (Promega, USA). Briefly, spheroids were collected along with 100 μL of the culture medium and transferred to a white 96-well platelet. Equivalent amounts (100 μL) of the kit's luminescent reagent were placed, and the plate was shaken for 5 min for cell lysis in an environment protected from light, and after 15 min, the plate was read in a luminescence reader at 560 nm.

To evaluate whether the formulation interfered with spheroid formation, a second set of plates was treated with the unloaded and fenretinide-loaded ME at IC_{15} (since it did not reduce spheroid viability) immediately after centrifugation. Spheroid formation and growth were documented using optical microscopy (EVOS AME-3302, USA) for 4 days, and size measurements were made in the ImageJ software.

2.8. Evaluation of *In Vivo* Formation and Ability to Prolong the Local Retention of a Fluorescent Marker. *2.8.1. Animals.* Sprague-Dawley female rats (6 weeks) from the Facility for SPF rat production at the Institute of Biomedical Sciences, Animal Facility Network, at the University of São Paulo were housed in the animal facility of the Department of Pharmacology with food and water *ad libitum*. The animal room was kept under a 12:12 h light−dark cycle (lights on at 7:00 am), and the temperature was maintained between 22 and 23 °C. The protocol was conducted in accordance with guidelines issued by the Brazilian Council for Control of Animal Experimentation (CONCEA) and approved by the Animal Care and Use Committee of the Institute of Biomedical Sciences at the University of São Paulo (number 4906211117). After reaching 6 weeks of age, animals were anaesthetized with isoflurane in oxygen (5% for induction and 2.5% for maintenance, Cristalia, Itapira, Brazil), and the hair from the abdomen was shaved using a depilatory cream applied for 50 s. The cream was rinsed off, and the animals were treated according to the experimental protocol. To ensure animal welfare, the rats were weighed periodically and the endpoints for the animals to be euthanized before the established 12 weeks were set: weight loss above 30%, the appearance of ulcers or skin lesions, palpable tumors above 50 mm^3, and behavioral changes that could indicate pain.[52]

2.8.2. Local Retention of the Formulation. This experiment aimed at assessing whether the selected ME formed a local depot that prolonged the release of a fluorescent marker. Alexa Fluor 647 was selected as the fluorescent marker because its emission wavelength is above 650 nm and thus is not subjected to interference of hair follicle autofluorescence.[36] The Alexa Fluor-loaded ME (0.05%, w/w) was obtained by diluting the marker in the polar phase of the formulation. A solution of the marker in PG (0.05%) was prepared as a control. To ensure that fluorescence was related to the presence of Alexa Fluor in the tissue, the unloaded ME was also administered as a control.

The precursor formulation was decontaminated by filtration through a poly(tetrafluoroethylene) (PTFE) filter (0.22 μm pore membranes, Pall, Acrodisc 4567) and administered in the mammary tissue, under the skin, in the inguinal region. Retention of the marker at the injection site was monitored using an *in vivo* image generation system (IVIS Spectrum, Core Facility for Scientific Research—University of Sao Paulo) 1 h and 3, 5, 14, 20, and 30 days after administration. The following instrument settings were fixed for comparison among groups: exposure time = 0.5 s, binning value = 8−2, excitation/emission = 640/780 nm. The fluorescence intensity at the injection site was determined by pixel counting using the IVIS software.[53] A selection tool from IVIS Spectrum software enabled the outlining of the fluorescent area (region of interest) to obtain the fluorescence intensity. The depot formed upon formulation administration was obtained after 3 h to assess whether lamellar phase formation occurred *in vivo*.

2.8.3. Local Irritation. To assess local irritation, the skin and mammary tissues adjacent to the application site were removed and embedded in paraffin, and histological sections were obtained to evaluate morphological changes. The sections were stained with hematoxylin and eosin for visualization of cell infiltration inflammatory diseases and changes in tissue architecture. The images were captured in a microscope attached to a desktop (Leica Microsystems DMC 2900, SP, Brazil) through the LAS V4.6 program (Leica Microsystems).

To further assess the formulation potential to cause local inflammation, myeloperoxidase (MPO) activity was assessed. MPO is an enzyme found in intracellular neutrophil granules, and it plays a role as a marker of recruitment of neutrophils at early time points.[54] The tissue of animals subjected to treatment for 3 h was removed and kept on dry ice for 30 min, and 100 mg of the sample was homogenized in Polytron for 15 s with 2 mL of hexadecyltrimethylammonium bromide buffer to obtain a homogenate that was then centrifuged for 10 min at 10,000*g* to collect 10 μL of the supernatant. Subsequently, 200 μL of *o*-dianisidine dihydrochloride was added to the supernatant, and absorbance was recorded at 460 nm every 15 s for 2 min at a UV−visible spectrophotometer. The MPO activity unit is defined as the one capable of degrading 1 μmol of H_2O_2 per minute at 25 °C.[55] Considering that the MPO unit is corrected by the amount of tissue sample (mg protein) as a function of absorbance unit (AU) and that 1 μmol of H_2O_2 corresponds to 0.0113, the following calculation results: MPO unit (U/mg) = change in absorbance (AU/min)/0.0113.

In addition, blood samples of each animal were collected in ethylenediaminetetraacetate tubes for white blood cell count in order to verify the systemic influence of the formulation.

2.9. Evaluation of the Formulation Efficiency in NMU-Induced Carcinogenesis Models. To assess the viability and effectiveness of the ME containing fenretinide, a model of chemically induced breast cancer in female Sprague-Dawley rats was used. Animals (8 weeks old) received a single intraperitoneal injection of 50 mg/kg of the *N*-nitrous-*N*-methylurea (NMU) direct-acting carcinogen to induce mammary tumors in the glands.[56,57] In control animals, saline was administered.

The animals were randomly divided into the following groups: (i) control (non-induced and untreated, C), (ii) induced but untreated (induced, I), (iii) induced and treated with the unloaded formulation (50 mg per breast, totaling 200 mg per animal, U-ME), and (iv) induced and treated with the fenretinide-loaded formulation (50 mg per breast, totaling 200 mg per animal, ME-F). Treatment was carried out as follows: 2 days before induction, the first treatment was performed by

https://doi.org/10.1021/acs.molpharmaceut.1c00319
Mol. Pharmaceutics 2021, 18, 3401−3417

injecting the formulations as described in the item "Local Retention of the Formulation". The same treatment protocol was conducted every 3 weeks until the 12th week, when the animals were euthanized. Subsequently, the breast tissue was removed and divided in three parts for (i) histological evaluation, (ii) evaluation of collagen expression, and (iii) quantification of fenretinide.

The tissue subjected to histological evaluation was fixed in 4% formaldehyde for 8 h at room temperature, processed, embedded in paraffin, and cut to 7 μm thick sections, which were positioned in glass slides and stained with hematoxylin and eosin. Histological changes in the duct structures (hypertrophy or epithelial hyperplasia, the presence of intraductal proliferation and desquamation of cells within the lumen), alveoli (the presence of hyperplastic alveolar nodules, with or without acidophilic secretion), and desmoplastic reaction (increased presence of fibroblasts, collagen, and cellular infiltrate) in the connective tissue around the ducts were assessed.

To determine the treatment's influence on the expression of collagen type I (thick fiber, stained in red) and collagen type III (thin fiber, stained in green) in cutaneous and mammary tissues, specimens were cut to 7 μm thick sections and stained with picrosirius red.

To establish relationships between the effect and fenretinide levels at the end of the efficacy assay both in the mammary tissue and in the plasma, the drug was quantified. Collected blood was processed as follows: whole blood was centrifuged at 773.6*g* for 30 min in order to separate the plasma, which was stored at −20 °C for a maximum of 3 days. The drug was extracted from plasma samples with acetonitrile (1:1 v/v, plasma/acetonitrile), followed by centrifugation at 3095*xg* for 15 min and filtration (PTFE filters, 0.45 μm pores) for HPLC analysis. The HPLC analytical method was adapted from Vaishampayan *et al.*[24] Briefly, the isocratic method uses a Phenomenex C-18 column (150 × 4.6 mm) and a mobile phase composed of acetonitrile/water/acetic acid (75:23:2, v/v/v), with injection of 20 μL to a flow rate 1 mL/min. The eluent was monitored at 365 nm for detection of the analyte. Calibration solutions of fenretinide were prepared in acetonitrile and plasma and demonstrated linearity within the range of 100−0.05 μg/mL (for acetonitrile solutions) and 50−0.5 μg/mL (for curves extracted from plasma). The limit of quantification was 50 ng/mL, and the detection limit was 10 ng/mL. The concentration of fenretinide in the analyzed tissues was determined based on the linear regression of the standard curve.

2.10. Statistical Analyses. The results are reported as means ± standard deviation (SD) or means ± standard error. Data were statistically analyzed using the ANOVA test, followed by the Tukey post-hoc test or *t*-test (session "Effects of the Formulation on Cell Viability") using GraphPad Prism software (Sand Diego, CA). Values were considered significantly different when $p < 0.05$.

3. RESULTS

3.1. Formulation Development and Characterization. Macroscopic analysis and polarized light microscopy demonstrated that several phases were formed upon addition of water at 2−90% to the non-aqueous ME containing 40% of PG (also referred to as 9:1−40%). Up to ∼30%, Maltese crosses and oily streaks were observed under the microscope, which are characteristic of the lamellar phase[58,59] (Figure 1A,B).

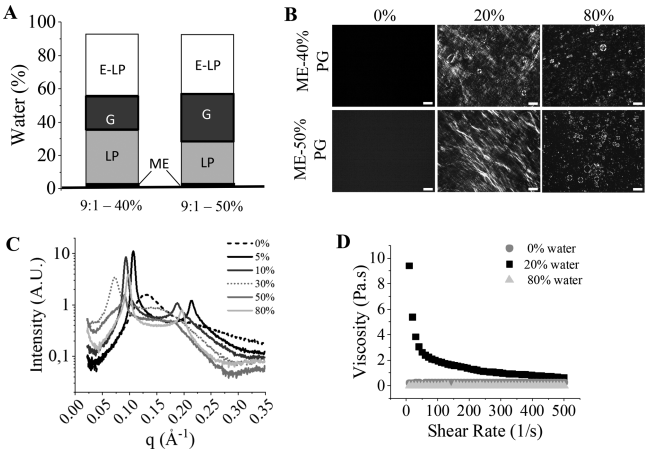

Figure 1. Formulation development and characterization. (A) Bar diagram of the phases formed by the MEs containing 40 and 50% of PG upon contact with water. Several phases were identified: (LP) lamellar, (G) amorphous gel, and (E-LP) lamellar phase-containing emulsion. As depicted, the lamellar phase exists over a narrower aqueous range in the formulation containing 50% of PG. (B) Representative images of polarized light optical microscopy of the formulation in contact with water. 20× magnification, bar = 50 μm. (C) SAXS patterns of unloaded formulations added or not with water 5% and up. (D) Viscosity of the ME (0% water) and its counterpart formulations containing 20 and 80% of water.

Increases of water up to ∼55% originated turbid gels without specific textures under the polarized light microscope. Further increases in the aqueous content led to the formation of emulsion-like systems (milky and visually less viscous than the gel) containing dispersed Maltese crosses, suggesting the presence of the lamellar phase in the aqueous phase of the system. This system was referred to as the lamellar phase-containing emulsion (E-LP, Figure 1A,B).

Increasing the percentage of PG from 40 to 50% (PC/T/PG, 45:5:50, w/w/w) reduced viscosity. Similar phases to those displayed by the 9:1−40% ME were observed as a function of the aqueous content, although the aqueous range in which the lamellar phase could be observed was reduced. This was not unexpected since PG reduces surface tension and has been described to influence the formation of liquid-crystalline phases in a concentration-dependent manner.[60−62] Similar transitions were observed when this ME was incubated at room temperature or 37 °C.

Because the ME containing PG at 50% was visually less viscous, which could facilitate injection, this formulation was selected for further studies. It displayed an average diameter of 175.3 ± 8.9 nm and a PDI of 0.106 ± 0.061, indicating a monodisperse sample (Supporting Information Figure S2).

To confirm the results from polarized light microscopy concerning phase behavior, a more in-depth characterization of the internal structure of the selected ME as a function of the aqueous content was provided by SAXS. The formation of an organized structure with 5 and 10% water was supported by the presence of two strong intensity and narrow width SAXS scattering peaks at the scattering curves, with q1/q2 of 1:2 being indicative of the lamellar structure[58] (Figure 1 and Table 1). At 30−50% of water, only one wide peak was observed, suggesting the formation of a disordered material, which supports macroscopic and polarized light microscopy observations of a gel without a specific texture. It is not clear why these gels were formed with ∼30−50% of water, but the need for

https://doi.org/10.1021/acs.molpharmaceut.1c00319
Mol. Pharmaceutics 2021, 18, 3401−3417

Table 1. SAXS of the Selected ME Containing Various Water Amounts[a]

water (%)	*d* (nm)	*hkl*	structure
0	4.83	(100)	isotropic
5	5.89	(100)	lamellar
	2.94	(200)	
10	6.75	(100)	lamellar
	3.35	(200)	
30	8.58	(100)	amorphous
50	6.9	(100)	amorphous
80	6.4	(100)	lamellar phase
	3.23	(200)	

[a](100) and (200) refer to the Miller indices and designate the plane of the crystallographic network.

longer times for equilibration, insufficient homogenization, and coexistence of multiple phases as previously described for other PC-based systems may have influenced the results.[63,64] At 80% of water, two strong intensity and narrow peaks (q1/q2 of 1:2) were again observed, suggesting the coexistence of lamellar phases in the emulsion-like system.

3.2. Influence of the Aqueous Content on the Rheological Behavior. To quantify differences in the viscosity of the systems observed as the content of water increased, the rheological behavior of formulations containing 0% (ME), 20%, and 80% of water was assessed. The ME presented Newtonian behavior, characterized by a constant viscosity at increasing rates of shear (Figure 1D). Its viscosity, calculated as the average of values at individual rates of shear, was 0.22 ± 0.01 Pa·s. The viscosity of the system containing 20% of water, which was characterized as the lamellar phase by polarized light microscopy and SAXS analysis, decreased with the rate of sheer, demonstrating pseudoplastic behavior (Figure 1D). At the lowest rate of shear employed, its viscosity was approximately 40-fold higher than that of the ME, which is consistent with its gel-like macroscopic appearance. A further increase in the aqueous content to 80% decreased the viscosity to levels similar to that of the ME, which is consistent with the formation of the more fluid, emulsion-like formulation.

3.3. Characterization of the ME Swelling and Spreading. Since the formulation undergoes phase transition upon incorporation of water, its swelling kinetics was assessed using 3% sodium alginate gel as the water donor to better mimic the environment of the nanomaterial in contact with the mammary tissue. The results revealed that water uptake was fast, reaching approximately 36.4% in 6 h; subsequently, a plateau was maintained (Figure 2A). A gel-like system was observed within 2 h of contact with fluids, and Maltese crosses with oily streaks were observed under a polarized light microscope, suggesting a relatively fast formation of the lamellar phase. After 24 h, a gel was observed macroscopically and only oily streaks (not Maltese crosses) were observed upon microscopic investigation. Although longer time points were not investigated, we anticipate reorganization of the system and the formation of the emulsion-like system as demonstrated by polarized light microscopy and SAXS analysis.

Percentages of water taken up by the formulation were fitted with three different kinetic models, and the results suggest that swelling can be better described by second-order kinetics (R^2 = 0.9995), which is similar to the results with liquid-crystalline-based systems[36,65,66] and indicates that swelling speed decreases proportionally to its uptake capacity and to the area that did not interact with the aqueous component.[67]

To try to predict whether the ME would spread quickly and widely when administered *in vivo*, we assessed the area

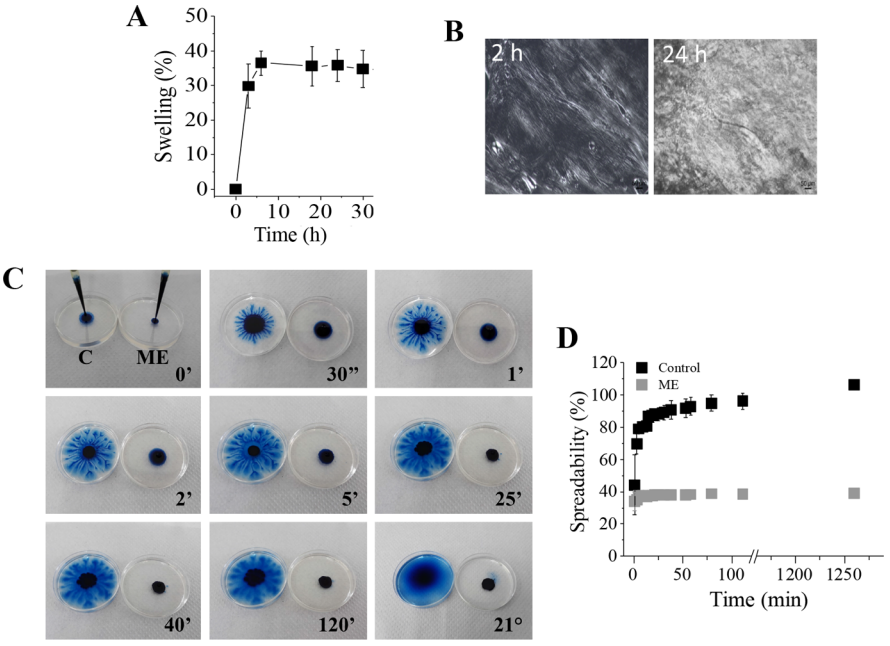

Figure 2. Swelling and spreadability of the formulation in the alginate gel. (A) Percentage of formulation swelling in the alginate gel as a function of time, shown as the mean ± SD of four replicates. (B) Representative images of polarized light microscopy of the formulation in contact with the alginate gel at 37 °C at 2−24 h. Magnification = 20×, bar: 50 μm. (C) Representation of the formulation (ME) spreading in the alginate gel (right) in comparison to the control (C) composed of a solution of Evans blue in PG (left) for up to 21 h. (D) Changes on the area occupied by the formulation as a function of time. Each point represents the mean ± SD of four replicates. It is possible to observe the great spread of PG in relation to the formulations.

https://doi.org/10.1021/acs.molpharmaceut.1c00319
Mol. Pharmaceutics 2021, 18, 3401−3417

resulting from the formulation spreading on top of a sodium alginate gel layer. We acknowledge the differences in the organization and composition of biological tissues compared to a flat layer of the gel, but this assay allowed us to study whether formulation spreading *in situ* would be prevented. As can be observed in Figure 2C, the Evan's blue dye solution in PG (employed as control) was capable of spreading throughout the surface of the gel, occupying the whole surface after 5 min. After contact of the selected ME with the gel, a noticeably lower area (5.1-fold) was observed, which did not increase after the initial 30 s. This demonstrates the ME ability to form a gel quickly after contact with the alginate gel (Figure 2D) and corroborates previous studies regarding the fast transition of other MEs intended for parenteral drug delivery.[43]

3.4. Fenretinide Incorporation and Release. No drug crystals were observed in the formulations when fenretinide was incorporated in the range of 1−5%. Additionally, phase transitions similar to those observed in the unloaded system upon contact with water were observed in the presence of fenretinide up to 5% (Supporting Information Figure S3).

Fenretinide release from the formulation increased with time, and at 72 h, approximately 15% of the drug was released (Supporting Information Figure S4). When a solution of the drug was employed as a control, approximately 100% of the drug was able to diffuse across the membrane in the same period, indicating that the membrane did not preclude drug release. On the last day of the experiment, approximately 30% of the drug's content was released. After data fitting and based on the highest values of the coefficient of determination obtained, release kinetics can be better described by the Higuchi model ($R^2 > 0.97$).

3.5. Cellular Effects of the Formulation. *3.5.1. Effects of the Formulation on Cell Viability.* To evaluate whether drug incorporation in the formulation affected its cytotoxicity, the viability of MCF-7 and T-47D after treatment with the selected ME was assessed. We obtained viability values exceeding 100% only in wells treated with the lowest concentrations of the unloaded ME or drug solution tested; the single-sample *t*-test indicated that these values were not different from 100%. Thus, we considered the maximum viability range of 100−120%. Viability values exceeding 100% have been reported for MTT, and the reasons include technical factors and experimental variability.[68]

The unloaded ME reduced the cell viability to values lower than 50% when used at 100 mg/mL and higher for both breast cancer cell lines (Figure 3A,B). Incorporation of fenretinide increased the cytotoxicity of the ME against both tumor cell lines, as evidenced by the shift of cell viability curves to the left (Figure 3A,B) and by the reduction of the formulation IC_{50} in comparison to the unloaded ME (Table 2).

Compared to the loaded ME, treatment of cancer cells with the fenretinide solution resulted in greater decreases on cell viability (Figure 3C,D). Because of the difference in the fenretinide concentration range, insets showing the viability curve resulting from treatment with the drug solution are depicted in Figure 3C,D. As a result, IC_{50} values of fenretinide solution in MCF-7 and T-47D were 68.3 and 13.2-fold lower, respectively, compared to ME-loaded treatment. The higher IC_{50} of the drug in the ME is consistent with the facts that (i) the formulation was not mixed with the culture medium but remained as a depot at the surface (as depicted in Supporting Information Figure S1) and (ii) the formulation was able to prolong drug release, resulting in less free drug available in the medium to elicit its effects.

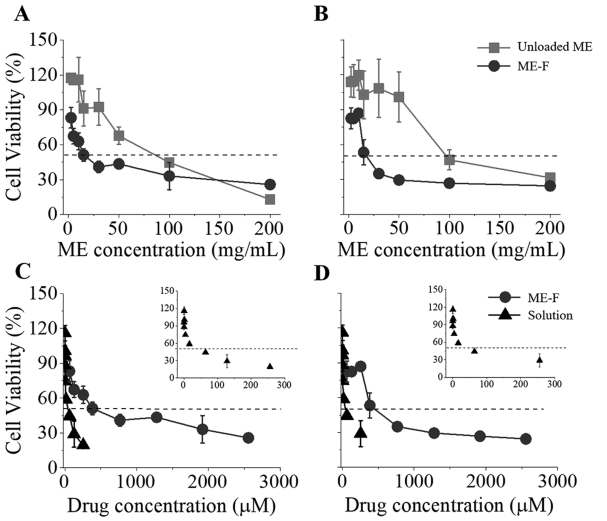

Figure 3. Influence of the concentration of unloaded, fenretinide-loaded ME, or fenretinide solution on the viability of MCF-7 and T-47D cells. (A,C) MCF-7 cells; (B,D) T-47D cells. (A,B) shows comparisons of the loaded and unloaded ME in MCF-7 and T-47D cells, respectively. (C,D) shows comparisons of fenretinide-loaded ME and the drug solution in MCF-7 and T-47D cells, respectively. Cell viability after treatment with fenretinide solution is also presented in the inset in (C,D) to enable better visualization of the relationship between concentration and viability. Data are represented as the mean ± SD, $n = 12-14$ in 3−4 separate experiments (each with 2−4 wells/treatment). The concentrations of the drug and formulation are presented in μM and mg/mL, respectively.

Table 2. IC_{50} Values of Fenretinide (μM, in Solution or in the ME) and the Formulation (mg/mL, Loaded or Unloaded) Determined in MCF-7 and T47-D Cells after 72 h of Treatment

treatment		cell type	
		MCF-7	T-47D
control solution	fenretinide (μM)	6.0	32.4
fenretinide-loaded ME		410.0	427.2
unloaded ME	formulation (mg/mL)	66.8	77.0
fenretinide-loaded ME		19.8	20.8

Comparing the effects of the drug between the two cell types, we observed that the IC_{50} of the fenretinide solution was higher in T-47D cells compared to MCF-7, suggesting that MCF-7 cells might be more susceptible to the effects of the drug (Table 2). This difference was not observed when the drug was incorporated in the ME, which again might result from the slower release. Because of the similarity of the drug-loaded ME effects on the two cell lines, we proceeded with T-47D cells only in further experiments.

3.5.2. Effects of the Formulation on Cell Migration. To evaluate the influence of the formulation on cell migration while avoiding a reduction in cell viability, the ME was employed at a concentration equivalent to the formulation IC_{15}. Treatment with the drug-loaded ME reduced cell migration by 75.9% ($p < 0.0001$) compared to untreated cells (Figure 4A,B). It is worth mentioning that the unloaded ME, employed at the same concentration of the fenretinide-loaded ME, also reduced cell migration (28.6%, $p < 0.01$),

https://doi.org/10.1021/acs.molpharmaceut.1c00319
Mol. Pharmaceutics 2021, 18, 3401−3417

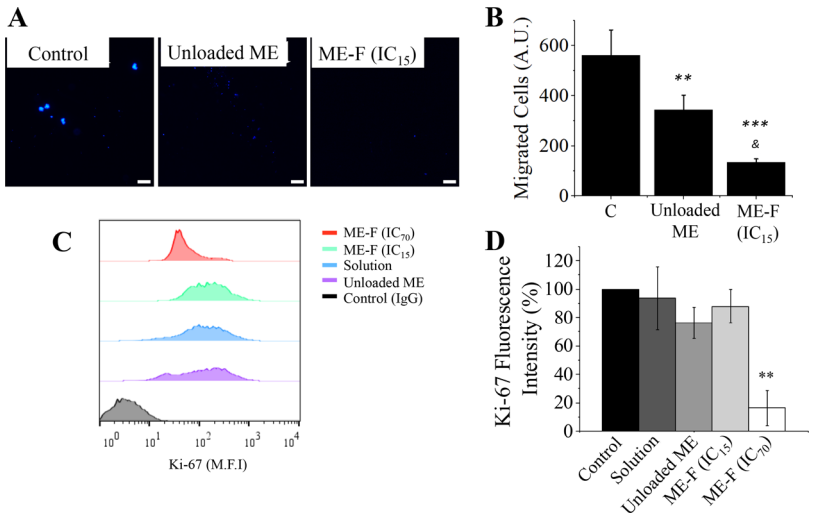

Figure 4. T-47D cell migration and Ki-67 in response to the unloaded and loaded formulations compared to control (untreated) cells. (A) Representative images of cells that migrated across the membrane after 24 h comparing untreated and treated cells with the unloaded formulation or ME containing fenretinide at concentrations equivalent to IC_{15}. Images were obtained under a fluorescence microscope after staining the cell nucleus with DAPI. Bar = 50 μm. (B) Treatment influence on the number of migrating cells. Tukey's statistical test ($n = 4$), where $^{**}p < 0.01$ and $^{***}p < 0.001$ compared to the control and $p < 0.05$ compared to the unloaded formulation. (C) Flow cytometry histogram comparing treatment influence on the expression of the Ki-67 proliferation marker on T-47D cells. (D) Ki-67 fluorescence intensity. Data are represented as the mean ± SD, $n = 5$. Tukey's statistical test; $^{**}p < 0.05$ compared to the control.

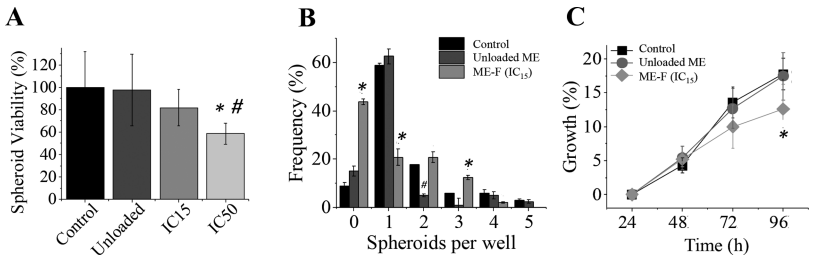

Figure 5. Influence of treatment on the spheroid formation, growth, and viability. (A) Spheroid viability. Tukey's statistical test, $^{*}p < 0.05$ compared to the untreated spheroids, $\#p < 0.05$ compared to the unloaded formulation, $n = 17-18$. (B) Distribution of the number of spheroids formed per well according to their respective treatments. Data are represented as the mean ± SD, $n = 13$. Tukey's statistical test, $^{*}p < 0.001$ compared to the control, $\#p < 0.001$ compared to loaded ME. (C) Spheroid size along 4 days. Data are represented as the mean ± SD, $n = 13-15$. Tukey's statistical test, $^{*}p < 0.05$ compared to the control.

although in a less pronounced manner. Nevertheless, this result is interesting and suggests that formulation components might help to prevent cell migration.

3.5.3. Effects of the Formulation on Cell Proliferation. To assess the ability of the formulation to interfere with proliferation pathways, the Ki-67 protein in treated cells was evaluated by flow cytometry. The unloaded and loaded ME at IC_{15} did not present pronounced antiproliferative effects compared to the untreated control (Figure 4C,D). A similar profile was also observed with fenretinide solution (employed at the IC_{15} determined for the solution). As a positive control for Ki-67 reduction, treatment with the formulation at the cytotoxic concentration of IC_{70} resulted in a decrease of approximately 84% in the proliferation rates.

3.6. Assessment of Formulation Effects on Spheroid Viability and Formation. We next assessed the ME effects on the viability, growth, and formation of spheroids, employed as 3D models of cancer. Treatment with the fenretinide-loaded ME at IC_{50}, but not at IC_{15}, significantly ($p < 0.05$) reduced spheroid viability compared to untreated and unloaded ME-treated samples (Figure 5A). The unloaded formulation (employed at the same amount as in the IC_{50} treatment) did not reduce spheroid viability, suggesting that the effect depends on the presence of fenretinide. Two conclusions can be drawn from these results: (i) fenretinide incorporation increased the cytotoxic effect of the formulation and (ii) as expected, higher formulation concentrations were necessary to reduce spheroid viability compared to cells in the monolayer since the IC_{50} determined in monolayers resulted in spheroid viability of ~65%.

Subsequently, we investigated whether the selected ME disrupted spheroid formation. Only one spheroid was formed in 62.5% of the wells treated with the unloaded ME (at the same amount employed in the IC_{15} treatment, Figure 5B). Since the method employed for spheroid production resulted in only one spheroid/well in ~61% of the wells in the absence of any treatment, we considered that the unloaded ME did not disrupt spheroid formation. On the other hand, treatment with the fenretinide-loaded ME resulted in one spheroid in ~20% of the wells and precluded the formation of spheroids (no spheroid formed) in 43.8% of the wells. In these wells, only very small aggregates and loose cells were observed. Therefore, compared to the untreated control, the loaded ME at IC_{15} significantly increased ($p < 0.001$) the number of wells without

https://doi.org/10.1021/acs.molpharmaceut.1c00319
Mol. Pharmaceutics 2021, 18, 3401−3417

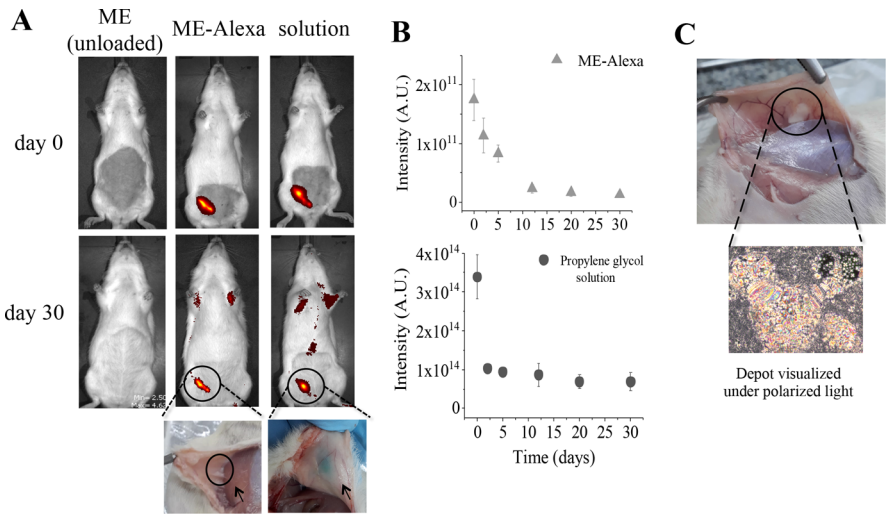

Figure 6. *In vivo* tissue retention of Alexa Fluor over 30 days. (A) Representative images of the fluorescence staining in animals treated with the unloaded ME, Alexa Fluor-loaded ME (ME-Alexa), or Alexa fluor solution in PG at days 0 (3 h after administration) and 30. Zoom: administration of Alexa fluor solution in the PG group resulted in tissue staining, suggesting that the fluorescent signal did not result from the presence of a formulation capable of prolonging release, while no tissue staining was observed after ME administration. The arrows point to formulation residue or tissue staining. (B) Changes in the intensity of fluorescence along 30 days after administration of the ME-Alexa or Alexa Fluor solution. It was not possible to distinguish the fluorescence from the skin and breast tissue in whole animal images; the overall intensity, without discriminating the skin and breast region, is depicted. Data are represented as the mean ± SD, $n = 3-4$ animals. (C) Formation of a depot after 3 h and its observation under polarized light microscopy.

spheroids and decreased ($p < 0.001$) the number of wells with only one spheroid, indicating that the presence of the drug affected the formation of these structures. Multiple (2−5) spheroids were observed less frequently (<20% of the wells).

Spheroid growth along time was calculated as the ratio of size at individual time points/sizes at 24 h. For this experiment, only the wells containing one spheroid were employed. After 4 days, spheroids treated with the fenretinide-loaded ME at IC_{15} displayed a lower size compared to those untreated or treated with the unloaded ME (a reduction of approximately 28.3% in size, $p < 0.05$) (Figure 5C). Treatment also appeared to reduce the growth rate, as demonstrated by a 1.4-fold lower slope of the growth curve of spheroids treated with fenretinide-loaded ME (an angular coefficient of 4.3) compared to untreated samples (6.3 and 6.0 for the control and unloaded ME, respectively).

3.7. *In Vivo* Formation and Ability to Prolong the Local Retention of a Fluorescent Marker. Formulation retention in the tissue and the presence of a fluorochrome (Alexa Fluor 647) over time were investigated using *in vivo* imaging. Administration of the unloaded ME produced no fluorescent staining, suggesting that any staining could be attributed to the presence of the fluorochrome (Figure 6A). ME loaded with Alexa Fluor (ME-Alexa) led to strong fluorescent staining of the area consistent with the mammary tissue, and despite the reduction of intensity and dimension of this area over time, staining could be detected at 30 days post application (Figure 6). As a control, a solution of Alexa Fluor in PG was administered and resulted in a strong fluorescent signal, even though no solution remained locally. This has been attributed to fluorochrome adsorption in the animal skin, which turned blue as shown in Figure 6. This retention was previously observed.[36] Although in whole animal fluorescence images it was not possible to distinguish the fluorescence in the breast tissue from that on the skin, administration of the Alexa-loaded ME did not result in blue stains in the skin (Figure 6). These results suggest that the formulation prevents prolonged adsorption to the skin, which is relevant to avert unwanted pharmacological effects of compounds that accumulate in this tissue. Of note, several lipophilic drugs tend to accumulate in the skin and its appendages, such as terbinafine.[69−71]

Although the selection of Alexa Fluor enabled us to avoid interference of hair follicles, unlike fenretinide, it is hydrophilic. Since lipophilicity has been described as one of the main correlates of *in vivo* volume of distribution (V_d), with V_d increasing with lipophilicity,[72] it is reasonable to expect that fenretinide might remain locally retained for longer periods of time compared to Alexa Fluor. Additionally, with the possibility of fenretinide slower dissolution in fluids *in vivo*, its tissue binding and accumulation in the breast and subcutaneous tissues support its longer retention.[17,22,27,73]

After 3 h of *in vivo* administration, it was possible to verify a local depot formed at the site of administration (Figure 6C). Under polarized light microscopy, it depicted a lamellar phase texture, suggesting that phase transformation was fast. After 30 days, a very small depot without a specific texture under the polarized light microscope was observed, which is consistent with phase transformation into a more fluid formulation as observed *in vitro*.

3.8. *In Vivo* Irritation. ME administration did not lead to changes in the tissue architecture compared to untreated animals or the appearance of inflammatory signals (such as edema and infiltration of inflammatory cells) in the areas surrounding the formulation, demonstrating that the characteristics of the breast tissue around the administration site were preserved (Figure 7A). In addition, the MPO activity assessment in the treated tissue showed that the formulation did not evoke irritating effects in the breast tissue; on the contrary, the MPO activity was significantly lower (1.6-fold, $p < 0.05$) than the control group (non-injected) (Figure 7B). The total leukocyte count in circulating blood evaluated at various time points after the injection did not reveal any

https://doi.org/10.1021/acs.molpharmaceut.1c00319
Mol. Pharmaceutics 2021, 18, 3401−3417

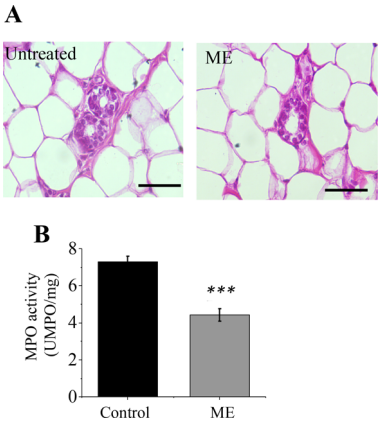

Figure 7. Formulation influence on local histological architecture and MPO quantification. (A) Representative image of the untreated tissue or after mammary administration of the unloaded ME obtained by optical microscopy. Bar: 50 μm. (B) Influence of mammary administration of the unloaded formulation on the MPO in units per mg of total protein observed at 3 h post application. n = 3; Tukey's statistical test, ***p < 0.001.

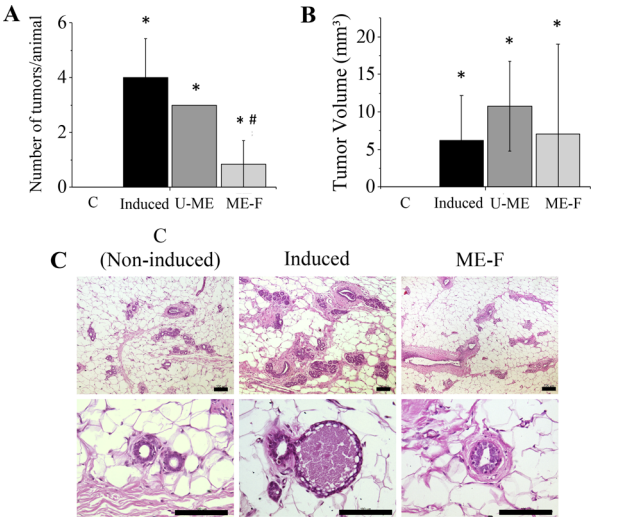

Figure 8. Effects of treatment of the chemically induced carcinogenesis *in vivo* model with the selected formulation. (A) Number of visible tumors comparing control animals [non-induced and untreated, (C)], those induced and untreated (induced), those induced and treated with the unloaded formulation (U-ME), and those induced and treated with the fenretinide-loaded formulation (ME-F). Data are represented as the mean ± SD, n = 3−7. Tukey's statistical test, *p < 0.05 compared to the control and #p < 0.05 compared to U-ME. (B) Volume of visible tumors related to treatment. Data are represented as the mean ± SD, n = 3−7. (C) Histology of the breast tissue. Bar = 100 μm.

significant changes resulting from the administration of the formulation (Supporting Information Table S1).

3.9. ME Efficacy *In Vivo* in NMU-Induced Carcinogenesis Models. No control animals (C, non-induced and untreated) developed palpable/visible tumors, while induced and untreated (induced) animals presented an average of ∼4 tumors/animal. A significant reduction (p < 0.05) on the number of tumors in the group treated with the fenretinide-loaded ME (ME-F) compared to induced and untreated animals (4.7-fold) and those treated with the unloaded ME (U-ME, 3.4-fold) was observed (Figure 8A), suggesting the efficacy of the loaded formulation to reduce tumor incidence. No significant difference was observed in the number of tumors comparing induced and untreated animals and those treated with the unloaded ME, demonstrating that the formulation effects can be attributed to fenretinide. A comparison of the volume of tumors revealed no difference among the groups (Figure 8B), suggesting that the formulation impacts incidence but not tumor dimensions if they arise. No animal presented a weight reduction superior to 9% along with treatment, but the weight of animals that were induced and untreated (induced) and treated with the unloaded formulation (U-ME) was lower (p < 0.05) compared to the non-induced group (C) (Supporting Information Figure S5); no weight loss was observed in the group treated with the fenretinide-loaded ME (ME-F).

The following characteristics were observed in the mammary tissue of the induced and untreated animals: ducts with hyperplastic stroma and desquamation of epithelial cells to the lumen, dilated alveoli with acidophilic secretion and stromal reaction, characterized by infiltration of immune cells and replacement of fat cells with fibroblasts and collagen fibers, in addition to cells in the process of cell death, indicating a degenerative process (Figure 8C). These characteristics support the ability of NMU to induce breast cancer. No control animals presented histological changes, while animals treated with fenretinide-loaded ME that developed tumors presented some of these histological alterations. Despite the presence of vacuoles, treatment with the drug-loaded ME reduced the presence of pyknotic cell nuclei and the ductal epithelium appeared more organized compared to the induced and untreated (I) group (Figure 8C).

Further insight into the impact of the fenretinide-loaded formulation on tissue organization was provided by picrosirius red staining. It revealed that animals that were induced and untreated (I) or treated with the unloaded formulation (U-ME) expressed lower type III collagen fibers in the cutaneous tissue compared to control animals (21 and 30%, respectively, p < 0.05) (Figure 9A,B), while in ME-F-treated animals, an increase in collagen type III values in cutaneous and mammary tissues was observed (p < 0.05 compared to C) (Figure 9A,C). Collagen type I did not appear to change.

Slight lymphocytopenia (a decrease of 10 and 12% in the number of lymphocytes approximately, related to the values obtained in control animals) and monocytosis (an approximately 2-fold increase of monocytes) were observed in the animals that were induced but untreated (I) or treated with the unloaded ME (U-ME) compared to control animals. This difference was not observed when control animals were compared to those treated with fenretinide-loaded ME (Supporting Information Table S2). A previous study hypothesized that the high level of monocytes might suppress the antitumor functions of T-cells, enabling cancer progression.[74] However, we found no supporting evidence of this effect in animal models of NMU-induced tumors.

To investigate whether the drug could be measured systemically in animals by the end of the treatment period, fenretinide was assessed in the plasma and breast tissue of animals. It is worth noting that we did not aim to perform a comprehensive PK/PD study but only to assess whether systemic levels were comparable to those in the mammary tissue. No drug was measured in the animals treated with the unloaded ME. Drug levels in the plasma of animals treated

https://doi.org/10.1021/acs.molpharmaceut.1c00319
Mol. Pharmaceutics 2021, 18, 3401−3417

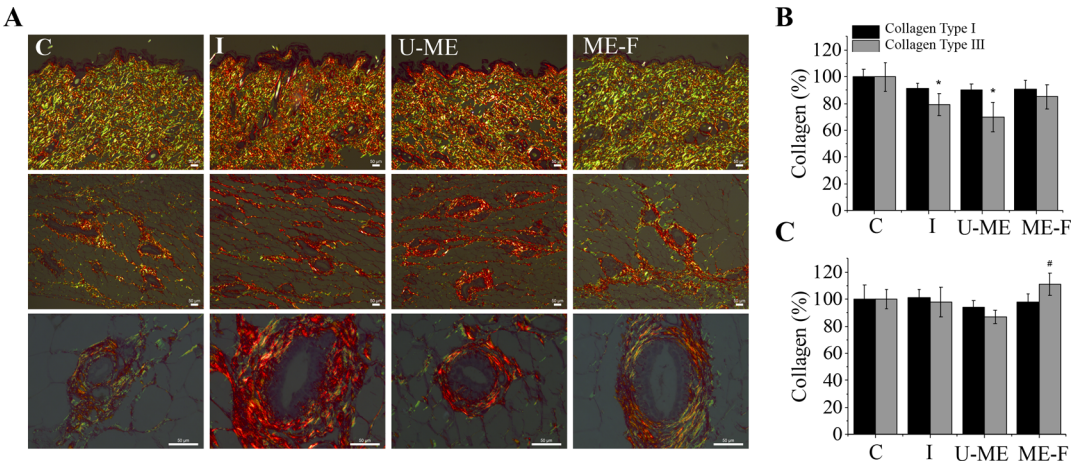

Figure 9. Influence of treatment on collagen type I and III in cutaneous and mammary tissues evidenced by picrosirius red staining. (A) Comparison of collagen type I and III in tissues of control animals [non-induced and untreated, (C)], those induced and untreated (I), those induced and treated with the unloaded formulation (U-ME), or those induced and treated with the fenretinide-loaded formulation (ME-F). Representative images of cutaneous (upper row) and mammary regions (10×—middle; 40×—bottom row). (B) Percentage of collagen I and III in the skin above the mammary tissue. Data are represented as the mean ± SD, $n = 3-7$. Tukey's statistical test, $^*p < 0.05$ compared to the control (C). (C) Percentage of collagen I and III in the mammary tissue. Data are represented as the mean ± SD, $n = 3-7$. Tukey's statistical test, $^*p < 0.05$ compared to the control (C).

with the fenretinide-loaded ME were below the detection limit of the method (which was 10 ng/mL), while an average of 1.3 ± 0.6 μg/mL of the drug was detected in the mammary tissue of treated animals after 30 days. These results support previous evidence that the drug can accumulate in the breast tissue and the potential applicability of this strategy to local chemoprevention.

4. DISCUSSION

In this study, a ME capable of gelling upon mammary administration to provide prolonged fenretinide release in the breasts was developed. In the first part of this study, development and characterization of the precursor ME, its transformation upon contact with water, and the relationship between composition and characteristics of the systems were described. Although the effects of fatty acids on PC phase behavior have been extensively studied, less attention has been granted to the influence of triglycerides.[63,75,76] Triglycerides are minor participants in membranes compared to fatty acids, but they have been reported to affect the physical properties of phospholipid membranes. Pakkanen *et al.* reported that mixtures of PC and triolein coexist as three macroscopical phases, a lamellar phase, a dilute vesicular phase, and an oil phase, and that triolein induced unique alterations in the membrane mechanical properties.[77] In this study, the formation of a lamellar phase in the presence of tricaprylin and PG was observed at a low aqueous content, while it coexisted with an emulsified system as the content of water increased above 60−70%. We were not able to characterize the structure of the gel observed between these two phases; the need for longer times for equilibration, insufficient homogenization, and coexistence of multiple phases as previously described for other delivery systems might help to justify this difficulty.[63,64]

When exposed to water, the selected ME underwent phase transition and was able to slow down fenretinide *in vitro* release; after 9 days, ∼30% of the drug was released following Higuchi's kinetics, which is in line with previous observations that assessed liquid-crystalline phases.[30,39,78,79] Although unexpected, this slow release might result from the high affinity of the drug to the formulation; even though the drug content could be dissolved in the receptor phase, its high lipophilicity and solubility in the formulation may have hindered its partition into the receptor phase. Drug release from liquid-crystalline systems and hydrogels may be influenced by several factors, including the internal structure, drug/matrix interactions, and physical−chemical characteristics (such as viscosity).[64] In addition to these factors, lipid-based systems have been demonstrated to undergo enzymatic degradation *in vivo*, affecting drug release. For example, monoacylglycerol-based liquid crystals are susceptible to lipolysis by a variety of enzymes, which attack the ester bond present on the lipid chain that links the acyl chain to the glycerol backbone, increasing drug release.[80] Considering that phospholipid-based carriers are also susceptible to enzymatic hydrolysis,[81] it would be reasonable to suggest that *in vivo* drug release from this formulation might be faster than *in vitro*;[82−86] however, fenretinide tissue binding and high lipophilicity (which has been suggested to delay its dissolution *in vivo*)[27] may further prolong its mammary tissue retention.

The prolonged drug release might help to justify the higher IC_{50} of the drug when incorporated in the selected ME compared to the drug solution, especially considering that the formulation was not mixed with the medium. A similar effect was observed by our group with alginate nanocarriers, which increased the MIC of miltefosine.[87] Other authors reported comparable effects of prolonged/controlled release systems, such as polymeric and calcium phosphate nanoparticles and liposomes, attributing increases of IC_{50} value to the reduced availability of the encapsulated drug.[88−94] Based on the *in vitro* release results, we estimate that free drug levels at 72 h should be approximately 15% of the total drug amount. Thus, if we consider that it is the free portion of the drug that will be available to exert cell effects, IC_{50} values would be lower.

Even with the increase in IC_{50}, the formulation was still able to prevent cell migration and interfere with spheroid formation at non-cytotoxic concentrations. Migration is an important factor in the development of cancer and its invasiveness.

https://doi.org/10.1021/acs.molpharmaceut.1c00319
Mol. Pharmaceutics 2021, 18, 3401−3417

Antimigratory effects of fenretinide have been attributed to the reduction of phosphorylation of FAK and AKT, proteins that control cell proliferation, angiogenesis, and metastasis and suppress the activation of NF-κB, an important transcription factor for tumor development and metastasis.[95−98] We also observed an effect of the unloaded formulation on cell viability and migration. Because the ME was placed above the cells for gel formation in the medium (and not in direct contact with the cells), we acknowledge the possibility of gel-related stress, interference with gas exchange, and release of components in the medium, affecting cell viability and migration. MEs have been demonstrated to influence cell and tissue viability depending on their composition since surfactants, lipids, and cosolvents may affect membrane fluidity and integrity, interfere with signaling pathways, and trigger the release of cytokines.[33,37,39,48,59,99−103] Although less studied, nanocarrier components might also affect cell migration. Short-chain triglycerides have been suggested to reduce cell viability and migration,[104,105] while a study carried out by Shin *et al.* demonstrated that liposomes inhibited the migration of SK-BR-3 cells by approximately 16.5%.[106]

The ability of fenretinide-loaded ME to reduce the number of spheroids/wells suggests interference with cell aggregation and supports previous observations that fenretinide disrupted spheroid formation in two medulloblastoma cell lines above 250 nM, most likely due to a decrease in the levels of the expression of CD133, ABCG2, Oct-4, and Sox-2, which are associated with *in vivo* tumor formation and development.[107] In addition, fenretinide-loaded ME also interfered with the T-47D spheroid growth rate, which is corroborated by Cuperus *et al.* previous results on neuroblastoma cells. The authors demonstrated that fenretinide at 1−10 μM reduced the growth rate and promoted cytostasis, possibly due to interference with PARP and Ki-67 pathways.[108,109] Another possible justification is that the phenomenon is a consequence of modulation of cell cycle-related factors, such as p16 and phospho-p38 MAPK.[25]

The increase in IC_{50} did not preclude *in vivo* efficacy as demonstrated by the 4.7-fold reduction in the *in vivo* incidence of tumors. This is consistent with previous clinical reports on the reduction of the incidence of second breast tumors in women[110] and provides additional support to the limitations of cell monolayers for efficacy studies. Additionally, the fact that treatment increased collagen type III expression in the mammary tissue further supports the formulation preventive potential given that (i) collagen type III appears to limit breast cancer progression and metastasis[111] and (ii) breast cancer is the most common neoplasia that metastasizes throughout the cutaneous tissue.[112,113] Evidence of the formulation safety is provided by the absence of changes on the tissue architecture upon ME administration by the reduction on NMU-induced weight loss and the absence of changes in the leukocyte count compared to the control animals. Fenretinide selectivity toward selected cancer cells may contribute to its overall safety. For example, at 5×10^{-6} M, fenretinide induced apoptosis and detachment of epidermoid carcinoma cells but not of dermal fibroblasts.[114] A reduction of the viability of the carcinoma 3D structures without affecting dermal fibroblasts was also demonstrated.[114] The cutaneous tolerability of fenretinide was further demonstrated in a clinical study: patients evaluated during and after 42 months of fenretinide oral intake at 200 mg/day showed mild signs of mucocutaneous dryness or skin atrophy, which are the main dermatological side effects associated with retinoids. In terms of the fenretinide effect on mammary tissue structures, orally treated rats showed a dose-dependent decrease in mammary gland ducts after 21 days,[115] decreased ductal branching, and end-bud proliferation relative to control glands 182 days after the first NMU injection,[17] which have been associated with its preventive effects. No longer-term studies detailing the effects of fenretinide in the breast tissue were available, but the results from a 15 year study suggest that oral fenretinide toxicity is manageable, with diminished dark adaptation and mild dermatological disorders as the main effects.[15]

Considering the low aqueous solubility and high tissue binding of the drug, a limitation of the present study is the absence of an additional control, consisting of the drug solution, in the *in vivo* efficacy study, which hinders a comparison of the ME efficacy to other conventional formulations and a more in-depth discussion on the *in vivo* prolonged release properties of the ME since drug tissue binding and diffusion from its biological reservoirs may affect its overall disposition.[27] Additionally, we have not investigated the distribution of fenretinide in the mammary tissue to determine whether it reaches the whole tissue homogeneously. Thorough tissue distribution of drugs locally delivered is restricted by a limited tissue penetration distance,[116] with solubilizers and permeation enhancers being proposed to increase tissue penetration.[22] Although fenretinide tissue distribution was not determined here, a previous study demonstrated a similar relative distribution of telapristone acetate across sampling sites in women breasts when administered topically to the breast skin compared to its oral administration,[28] with subcutaneous fat and deep (closer to muscles) sites having the highest concentration. The authors suggested that the fatty envelope of the breast might serve as a reservoir for prolonged drug distribution aided by the mammary lymphatic circulation. Despite differences in fenretinide and telapristone acetate characteristics, this previous study indicates that administration close to the mammary tissue may enable a similar pattern of mammary tissue distribution to oral delivery with lower systemic levels. Future studies should evaluate fenretinide distribution in the breasts.

Despite these limitations, the results presented here demonstrated that the ME administration reduced the incidence of breast cancer, which indicates the potential applicability of this strategy. The fact that few tumors were still observed in the ferentinide-loaded ME-treated animals points to the benefit of optimizing dosage and administration frequency so that we can maximize the treatment ability to prevent tumor development with the least number of applications, contributing to improve patient adherence to treatment.

5. CONCLUSIONS

In this study, we developed a non-aqueous precursor ME capable of phase transformation upon uptake of fluids to provide prolonged fenretinide release. Despite the increased IC_{50} value resulting from fenretinide incorporation, which we attributed to the formation of a depot and slow release, the formulation reduced cell migration and interfered with spheroids formation *in vitro*, supporting preventive effects. Consistent with these effects, the formulation reduced the incidence of tumors in an *in vivo* chemical carcinogenesis breast cancer model, without producing local irritation, changes in the tissue architecture at the vicinity of the

https://doi.org/10.1021/acs.molpharmaceut.1c00319
Mol. Pharmaceutics 2021, 18, 3401−3417

injection site, or systemic alterations in white blood cell count. The benefits of the formulation were also demonstrated by the prevention of weight loss in the treated animals and increases in type III collagen expression in the mammary tissue, which support its contribution to limiting the disease development and spreading. With this study, we aimed at contributing to the development of an effective, safe, and much needed preventive strategy for breast cancer.

■ ASSOCIATED CONTENT

Supporting Information

The Supporting Information is available free of charge at https://pubs.acs.org/doi/10.1021/acs.molpharmaceut.1c00319.

Representation of the experimental setup of the *in vitro* cytotoxicity assay and additional experimental results (PDF)

■ AUTHOR INFORMATION

Corresponding Author

Luciana B. Lopes − *Departamento de Farmacologia, Instituto de Ciências Biomédicas, Universidade de São Paulo, São Paulo, São Paulo 05508-000, Brazil;* orcid.org/0000-0001-7814-9647; Phone: 55 11 30917317; Email: lublopes@usp.br

Authors

Giovanna Cassone Salata − *Departamento de Farmacologia, Instituto de Ciências Biomédicas, Universidade de São Paulo, São Paulo, São Paulo 05508-000, Brazil;* orcid.org/0000-0001-6718-6602

Isabella D. Malagó − *Departamento de Farmacologia, Instituto de Ciências Biomédicas, Universidade de São Paulo, São Paulo, São Paulo 05508-000, Brazil*

Vanessa F. M. Carvalho Dartora − *Departamento de Farmacologia, Instituto de Ciências Biomédicas, Universidade de São Paulo, São Paulo, São Paulo 05508-000, Brazil*

Ana Flávia Marçal Pessoa − *Departamento de Cirurgia, LIM26, Faculdade de Medicina, Universidade de São Paulo, São Paulo, São Paulo 01246903, Brazil*

Márcia Carvalho de Abreu Fantini − *Departamento de Física Aplicada, Instituto de Física, Universidade de São Paulo, São Paulo, São Paulo 05508-090, Brazil*

Soraia K. P. Costa − *Departamento de Farmacologia, Instituto de Ciências Biomédicas, Universidade de São Paulo, São Paulo, São Paulo 05508-000, Brazil*

João Agostinho Machado-Neto − *Departamento de Farmacologia, Instituto de Ciências Biomédicas, Universidade de São Paulo, São Paulo, São Paulo 05508-000, Brazil*

Complete contact information is available at: https://pubs.acs.org/10.1021/acs.molpharmaceut.1c00319

Notes

The authors declare the following competing financial interest(s): The authors filed a patent application in Brazil related to the study. It is currently pending.

■ ACKNOWLEDGMENTS

The authors would like to thank Moacir de Britto and Dr. Simone Teixeira for technical support. This research was supported by the São Paulo Research Foundation (FAPESP, grants #2017/23213-0; #2008/52084-5, #2018/13877-1, 2016/06146-5, and #2019/23864-7), the Brazilian Council for Research (CNPq, grant #402613/2007-4), the Brazilian Federal Agency for Support and Evaluation of Graduate Education (CAPES, finance code 001), and the Royal Society (2016/R1 Newton Grant—eGAP SZ50730). MCAF, S.K.P.C., and L.B.L. are recipients of CNPq fellowships (#302468/2017-0, #312514/2019-0, and #306866/2020-0). This study is part of the National Institute of Science and Technology in Pharmaceutical Nanotechnology: a transdisciplinary approach INCT-NANOFARMA, which is supported by FAPESP (grant #2014/50928-2) and CNPq (grant #465687/2014-8).

■ REFERENCES

(1) Bernard, W. S.; Christopher, P. W. *World Cancer Report World Health Organization*, 2014.

(2) Bray, F.; Ferlay, J.; Soerjomataram, I.; Siegel, R. L.; Torre, L. A.; Jemal, A. Global Cancer Statistics 2018: GLOBOCAN Estimates of Incidence And Mortality Worldwide for 36 Cancers in 185 Countries. *Ca-Cancer J. Clin.* **2018**, *68*, 394−424.

(3) Waters, E. A.; McNeel, T. S.; Stevens, W. M.; Freedman, A. N. Use of Tamoxifen and Raloxifene for Breast Cancer Chemoprevention in 2010. *Breast Canc. Res. Treat.* **2012**, *134*, 875−880.

(4) Khan, S. A.; Hernandez-Villafuerte, K. V.; Muchadeyi, M. T.; Schlander, M. Cost-Effectiveness of Risk-Based Breast Cancer Screening: A Systematic Review. *Int. J. Cancer* **2021**, DOI: 10.1002/ijc.33593. In press

(5) Vogel, V. G. Implementation of Risk-reducing Strategies for Breast Cancer is Long Overdue. *Canc. Prev. Res.* **2021**, *14*, 1−4.

(6) Lee, O.; Khan, S. A. Novel Routes for Administering Chemoprevention: Local Transdermal Therapy to the Breasts. *Semin. Oncol.* **2016**, *43*, 107−115.

(7) Roche, C. A.; Tang, R.; Coopey, S. B.; Hughes, K. S. Chemoprevention Acceptance and Adherence in Women With High-Risk Breast Lesions. *Breast J.* **2019**, *25*, 190−195.

(8) Kroemeke, A.; Bargiel-Matusiewicz, K.; Kalamarz, M. Mixed Psychological Changes Following Mastectomy: Unique Predictors and Heterogeneity of Post-Traumatic Growth and Post-Traumatic Depreciation. *Front. Psychol.* **2017**, *8*, 1245.

(9) Lloyd, K. E.; Hall, L. H.; Ziegler, L.; Smith, S. G. Breast Cancer Worry Ii Higher-Risk Women Offered Preventive Therapy: A UK Multicentre Prospective Study. *Breast Canc. Res. Treat.* **2021**, *188*, 703−712.

(10) Cowan, A. J.; Frayo, S. L.; Press, O. W.; Palanca-Wessels, M. C.; Pagel, J. M.; Green, D. J.; Gopal, A. K. Bortezomib and Fenretinide Induce Synergistic Cytotoxicity in Mantle Cell Lymphoma Via Apoptosis, Cell Cycle Dysregulation, and Iκbα Kinase Down-Regulation. *Anti Canc. Drugs* **2015**, *26*, 974.

(11) Ulukaya, E.; Sarimahmut, M.; Cevatemre, B.; Ari, F.; Yerlikaya, A.; Dimas, K. Additive Enhancement of Apoptosis by TRAIL and Fenretinide in Metastatic Breast Cancer Cells in Vitro. *Biomed. Pharmacother.* **2014**, *68*, 477−482.

(12) Shishodia, S.; Gutierrez, A. M.; Lotan, R.; Aggarwal, B. B. N-(4-hydroxyphenyl)retinamide Inhibits Invasion, Suppresses Osteoclastogenesis, and Potentiates Apoptosis Through Down-Regulation of I(Kappa)B(Alpha) Kinase and Nuclear Factor-Kappab-Regulated Gene Products. *Cancer Res.* **2005**, *65*, 9555−9565.

(13) Wu, J. M.; DiPietrantonio, A. M.; Hsieh, T.-C. Mechanism of Fenretinide (4-HPR)-Induced Cell Death. *Apoptosis* **2001**, *6*, 377−388.

(14) Hail, N.; Kim, H. J.; Lotan, R. Mechanisms of fenretinide-Induced Apoptosis. *Apoptosis* **2006**, *11*, 1677−1694.

(15) Veronesi, U.; Mariani, L.; Decensi, A.; Formelli, F.; Camerini, T.; Miceli, R.; Di Mauro, M. G.; Costa, A.; Marubini, E.; Sporn, M. B.; De Palo, G. Fifteen-year Results of a Randomized Phase III Trial of Fenretinide to Prevent Second Breast Cancer. *Ann. Oncol.* **2006**, *17*, 1065−1071.

(16) Rotmensz, N.; De Palo, G.; Formelli, F.; Costa, A.; Marubini, E.; Campa, T.; Crippa, A.; Danesini, G. M.; Delle Grottaglie, M.; Di

Mauro, M. G.; Filiberti, A.; Gallazzi, M.; Guzzon, A.; Magni, A.; Malone, W.; Mariani, L.; Palvarini, M.; Perloff, M.; Pizzichetta, M.; Veronesi, U. Long-term Tolerability of Fenretinide (4-HPR) in Breast Cancer Patients. *Eur. J. Canc.* **1991**, *27*, 1127−1131.
(17) Moon, R. C.; Thompson, H. J.; Becci, P. J.; Grubbs, C. J.; Gander, R. J.; Newton, D. L.; Smith, J. M.; Phillips, S. L.; Henderson, W. R.; Mullen, L. T.; Brown, C. C.; Sporn, M. B. N-(4-Hydroxyphenyl)retinamide, a New Retinoid For Prevention of Breast Cancer in the Rat. *Cancer Res.* **1979**, *39*, 1339−1346.
(18) Mehta, R. G.; Moon, R. C.; Hawthorne, M.; Formelli, F.; Costa, A. Distribution of fenretinide in the Mammary Gland of Breast Cancer Patients. *Eur. J. Canc.* **1991**, *27*, 138−141.
(19) Sabichi, A. L.; Modiano, M. R.; Lee, J. J.; Peng, Y. M.; Xu, M. J.; Villar, H.; Dalton, W. S.; Lippman, S. M. Breast Tissue Accumulation of Retinamides in a Randomized Short-term Study of Fenretinide. *Clin. Cancer Res.* **2003**, *9*, 2400.
(20) Formelli, F.; Clerici, M.; Campa, T.; Di Mauro, M. G.; Magni, A.; Mascotti, G.; Moglia, D.; De Palo, G.; Costa, A.; Veronesi, U. Five-year Administration of Fenretinide: Pharmacokinetics and Effects on Plasma Retinol Concentrations. *J. Clin. Oncol.* **1993**, *11*, 2036−2042.
(21) Formelli, F.; Carsana, R.; Costa, A.; Buranelli, F.; Campa, T.; Dossena, G.; Magni, A.; Pizzichetta, M. Plasma Retinol Level Reduction by the Synthetic Retinoid Fenretinide: A One Year Follow-up Study of Breast Cancer Patients. *Cancer Res.* **1989**, *49*, 6149−6152.
(22) Nieto, K. J. *Long-Acting Release Implants for Local Fenretinide Delivery and Oral Cancer Chemoprevention*; University of Michigan, 2017.
(23) Veronesi, U.; De Palo, G.; Marubini, E.; Costa, A.; Formelli, F.; Mariani, L.; Decensi, A.; Camerini, T.; Del Turco, M. R.; Di Mauro, M. G.; Muraca, M. G.; Del Vecchio, M.; Pinto, C.; D'Aiuto, G.; Boni, C.; Campa, T.; Magni, A.; Miceli, R.; Perloff, M.; Malone, W. F.; Sporn, M. B. Randomized Trial of Fenretinide to Prevent Second Breast Malignancy in Women With Early Breast Cancer. *J. Natl. Cancer Inst.* **1999**, *91*, 1847−1856.
(24) Vaishampayan, U.; Heilbrun, L. K.; Parchment, R. E.; Jain, V.; Zwiebel, J.; Boinpally, R. R.; LoRusso, P.; Hussain, M. Phase II Trial of Fenretinide in Advanced Renal Carcinoma. *Invest. New Drugs* **2005**, *23*, 179−185.
(25) Orienti, I.; Francescangeli, F.; De Angelis, M. L.; Bongiorno-Borbone, L.; Signore, M.; Peschiaroli, A.; Boe, A.; Bruselles, A.; Costantino, A.; Eramo, A.; Salvati, V.; Sette, G.; Contavalli, P.; Zolla, L.; Oki, T.; Kitamura, T.; Spada, M.; Giuliani, A.; Baiocchi, M.; La Torre, F.; Melino, G.; Tartaglia, M.; De Maria, R.; Zeuner, A. A New Bioavailable Fenretinide Formulation with Antiproliferative, Antimetabolic, and Cytotoxic Effects on Solid Tumors. *Cell Death Dis.* **2019**, *10*, 529.
(26) Zhang, Y.; Wischke, C.; Mittal, S.; Mitra, A.; Schwendeman, S. P. Design of Controlled Release PLGA Microspheres for Hydrophobic Fenretinide. *Mol. Pharm.* **2016**, *13*, 2622−2630.
(27) Nieto, K.; Pei, P.; Wang, D.; Mallery, S. R.; Schwendeman, S. P. In Vivo Controlled Release of Fenretinide from Long-Acting Release Depots for Chemoprevention of Oral Squamous Cell Carcinoma Recurrence. *Int. J. Pharm.* **2018**, *538*, 48−56.
(28) Lee, O.; Pilewskie, M.; Karlan, S.; Tull, M. B.; Benante, K.; Xu, Y.; Blanco, L.; Helenowski, I.; Kocherginsky, M.; Yadav, S.; Hosseini, O.; Hansen, N.; Bethke, K.; Muzzio, M.; Troester, M. A.; Dimond, E.; Perloff, M.; Heckman-Stoddard, B.; Khan, S. A. Local Transdermal Delivery of Telapristone Acetate Through Breast Skin, Compared With Oral Treatment: A Randomized Double-Blind, Placebo-Controlled Phase II Trial. *Clin. Pharmacol. Ther.* **2021**, *109*, 728−738.
(29) Patel, N.; Schmid, U.; Lawrence, M. J. Phospholipid-based Microemulsions Suitable for Use in Foods. *J. Agric. Food Chem.* **2006**, *54*, 7817−7824.
(30) Hosmer, J. M.; Shin, S. H.; Nornoo, A.; Zheng, H.; Lopes, L. B. Influence of Internal Structure and Composition of Liquid Crystalline Phases on Topical Delivery of Paclitaxel. *J. Pharm. Sci.* **2011**, *100*, 1444−1455.
(31) Carvalho, V. F. M.; Salata, G. C.; de Matos, J. K. R.; Costa-Fernandez, S.; Chorilli, M.; Steiner, A. A.; de Araujo, G. L. B.; Silveira, E. R.; Costa-Lotufo, L. V.; Lopes, L. B. Optimization of Composition And Obtainment Parameters of Biocompatible Nanoemulsions Intended for Intraductal Administration of Piplartine (Piperlongumine) and Mammary Tissue Targeting. *Int. J. Pharm.* **2019**, *567*, 118460.
(32) Chhabra, R. P. Non-Newtonian fFuids: An Introduction. *Rheology of Complex Fluids*; Springer, 2010; pp 3−34.
(33) Carvalho, V. F.; de Lemos, D. P.; Vieira, C. S.; Migotto, A.; Lopes, L. B. Potential of Non-aqueous Microemulsions to Improve the Delivery of Lipophilic Drugs to the Skin. *AAPS PharmSciTech* **2017**, *18*, 1739−1749.
(34) Lawrence, M. J.; Rees, G. D. Microemulsion-based Media as Novel Drug Delivery Systems. *Adv. Drug Deliv. Rev.* **2012**, *64*, 175−193.
(35) Lopes, L. B. Overcoming the Cutaneous Barrier with Microemulsions. *Pharmaceutics* **2014**, *6*, 52−77.
(36) Santos, R. A.; Rae, M.; Dartora, V. F. M. C.; Matos, J. K. R.; Camarini, R.; Lopes, L. B. Bioresponsive Nanostructured Systems for Sustained Naltrexone Release and Treatment of Alcohol Use Disorder: Development and Biological Evaluation. *Int. J. Pharm.* **2020**, *585*, 119474.
(37) Pepe, D.; McCall, M.; Zheng, H.; Lopes, L. B. Protein Transduction Domain-Containing Microemulsions as Cutaneous Delivery Systems For an Anticancer Agent. *J. Pharm. Sci.* **2013**, *102*, 1476−1487.
(38) Apolinário, A. C.; Hauschke, L.; Nunes, J. R.; Lopes, L. B. Lipid Nanovesicles for Biomedical Applications: 'What is in a Name'? *Prog. Lipid Res.* **2021**, *82*, 101096.
(39) Phelps, J.; Bentley, M. V. L. B.; Lopes, L. B. In situ Gelling Hexagonal Phases for Sustained Release of an Anti-Addiction Drug. *Colloids Surf., B* **2011**, *87*, 391−398.
(40) Pollack, G. H. *Cells, Gels and the Engines of Life: A New, Unifying Approach to Cell Biology*; Ebner and Sons, 2001; p 320.
(41) Serban, M. A.; Liu, Y.; Prestwich, G. D. Effects of Extracellular Matrix Analogues on Primary Human Fibroblast Behavior. *Acta Biomater.* **2008**, *4*, 67−75.
(42) Schott, H. Kinetics of swelling of polymers and their gels. *J. Pharm. Sci.* **1992**, *81*, 467−470.
(43) Ren, X.; Svirskis, D.; Alany, R. G.; Zargar-Shoshtari, S.; Wu, Z. In-situ Phase Transition From Microemulsion to Liquid Crystal With the Potential of Prolonged Parenteral Drug Delivery. *Int. J. Pharm.* **2012**, *431*, 130−137.
(44) Desai, K.-G. H.; Mallery, S. R.; Holpuch, A. S.; Schwendeman, S. P. Development and in Vitro-In Vivo Evaluation Of Fenretinide-Loaded Oral Mucoadhesive Patches For Site-Specific Chemoprevention Of Oral Cancer. *Pharm. Res.* **2011**, *28*, 2599−2609.
(45) Dash, S.; Murthy, P. N.; Nath, L.; Chowdhury, P. Kinetic Modeling on Drug Release from Controlled Drug Delivery Systems. *Acta Pol. Pharm.* **2010**, *67*, 217−223.
(46) Allison, K. H.; Hammond, M. E. H.; Dowsett, M.; McKernin, S. E.; Carey, L. A.; Fitzgibbons, P. L.; Hayes, D. F.; Lakhani, S. R.; Chavez-MacGregor, M.; Perlmutter, J.; Perou, C. M.; Regan, M. M.; Rimm, D. L.; Symmans, W. F.; Torlakovic, E. E.; Varella, L.; Viale, G.; Weisberg, T. F.; McShane, L. M.; Wolff, A. C. Estrogen and Progesterone Receptor Testing in Breast Cancer: American Society of Clinical Oncology/College of American Pathologists Guideline Update. *Arch. Pathol. Lab Med.* **2020**, *144*, 545−563.
(47) Mooney, L. M.; Al-Sakkaf, K. A.; Brown, B. L.; Dobson, P. R. M. Apoptotic Mechanisms in T47D and MCF-7 Human Breast Cancer Cells. *Br. J. Canc.* **2002**, *87*, 909−917.
(48) Pepe, D.; Carvalho, V. F.; McCall, M.; de Lemos, D. P.; Lopes, L. B. Transportan in Nanocarriers Improves Skin Localization and Antitumor Activity of Paclitaxel. *Int. J. Nanomed.* **2016**, *11*, 2009−2019.
(49) Salata, G. C.; Pinho, C. F.; de Freitas, A. T. A. G.; Aquino, A. M.; Justulin, L. A.; Mendes, L. O.; Gonçalves, B. F.; Delella, F. K.; Scarano, W. R. Raloxifene Decreases Cell Viability And Migratory

https://doi.org/10.1021/acs.molpharmaceut.1c00319
Mol. Pharmaceutics 2021, 18, 3401−3417

Potential In Prostate Cancer Cells (LNCaP) with GPR30/GPER1 Involvement. *J. Pharm. Pharmacol.* **2019**, *71*, 1065−1071.
(50) Machado-Neto, J. A.; de Melo Campos, P.; Favaro, P.; Lazarini, M.; da Silva Santos Duarte, A.; Lorand-Metze, I.; Costa, F. F.; Olalla Saad, S. T.; Traina, F. Stathmin 1 Inhibition Amplifies Ruxolitinib-Induced Apoptosis in JAK2V617F cells. *Oncotarget* **2015**, *6*, 29573.
(51) Bussador do Amaral, J.; Shiniti Urabayashi, M.; Maria Machado-Santelli, G. Cell death and lumen formation in spheroids of MCF-7 cells. *Cell Biol. Int.* **2010**, *34*, 267−274.
(52) Workman, P.; Aboagye, E. O.; Aboagye, E. O.; Balkwill, F.; Balmain, A.; Bruder, G.; Chaplin, D. J.; Double, J. A.; Everitt, J.; Farningham, D. A. H.; Glennie, M. J.; Kelland, L. R.; Robinson, V.; Stratford, I. J.; Tozer, G. M.; Watson, S.; Wedge, S. R.; Eccles, S. A. Guidelines for the Welfare and Use of Animals in Cancer Research. *Br. J. Canc.* **2010**, *102*, 1555.
(53) Migotto, A.; Carvalho, V. F. M.; Salata, G. C.; da Silva, F. W. M.; Yan, C. Y. I.; Ishida, K.; Costa-Lotufo, L. V.; Steiner, A. A.; Lopes, L. B. Multifunctional Nanoemulsions for Intraductal Delivery as a New Platform for Local Treatment Of Breast Cancer. *Drug Deliv.* **2018**, *25*, 654−667.
(54) Herrera, B. S.; Martins-Porto, R.; Campi, P.; Holzhausen, M.; Teixeira, S. A.; Mendes, G. D.; Costa, S. K. P.; Gyurko, R.; Van Dyke, T. E.; Spolidório, L. C.; Muscará, M. N. Local and Cardiorenal Effects of Periodontitis in Nitric Oxide-Deficient Hypertensive Rats. *Arch. Oral Biol.* **2011**, *56*, 41−47.
(55) Bradley, P.; Christensen, R.; Rothstein, G. Cellular and Extracellular Myeloperoxidase in Pyogenic Inflammation. *Blood* **1982**, *60*, 618−622.
(56) Rivera, E. S.; Andrade, N.; Martin, G.; Melito, G.; Cricco, G.; Mohamad, N.; Davio, C.; Caro, R.; Bergoc, R. M. Induction of Mammary Tumors in Rat by Intraperitoneal Injection of NMU: Histopathology and Estral Cycle Influence. *Canc. Lett.* **1994**, *86*, 223−228.
(57) Murray, T. J.; Ucci, A. A.; Maffini, M. V.; Sonnenschein, C.; Soto, A. M. Histological Analysis of Low Dose NMU Effects in the Rat Mammary Gland. *BMC Canc.* **2009**, *9*, 267.
(58) Gosenca, M.; Bešter-Rogač, M.; Gašperlin, M. Lecithin-based Lamellar Liquid Crystals as a Physiologically Acceptable Dermal Delivery System for Ascorbyl Palmitate. *Eur. J. Pharm. Sci.* **2013**, *50*, 114−122.
(59) Hosmer, J. M.; Steiner, A. A.; Lopes, L. B. Lamellar Liquid Crystalline Phases for Cutaneous Delivery of Paclitaxel: Impact of the Monoglyceride. *Pharm. Res.* **2013**, *30*, 694−706.
(60) Alfons, K.; Engstrom, S. Drug Compatibility With The Sponge Phases Formed In Monoolein, Water,aAnd Propylene Glycol or Poly(ethylene glycol). *J. Pharm. Sci.* **1998**, *87*, 1527−1530.
(61) Ivanova, R.; Lindman, B.; Alexandridis, P. Effect of Glycols on the Self-Assembly of Amphiphilic Block Copolymers in Water. 1. Phase Diagrams and Structure Identification. *Langmuir* **2000**, *16*, 3660−3675.
(62) Engström, S.; Wadsten-Hindrichsen, P.; Hernius, B. Cubic, Sponge, and Lamellar Phases in the Glyceryl Monooleyl Ether−Propylene Glycol−Water System. *Langmuir* **2007**, *23*, 10020−10025.
(63) Godoy, C. A.; Valiente, M.; Pons, R.; Montalvo, G. Effect of Fatty Acids on Self-Assembly of Soybean Lecithin Systems. *Colloids Surf., B* **2015**, *131*, 21−28.
(64) Lopes, L. B.; Lopes, J. L. C.; Oliveira, D. C. R.; Thomazini, J. A.; Garcia, M. T. J.; Fantini, M. C. A.; Collett, J. H.; Bentley, M. V. L. B. Liquid Crystalline Phases of Monoolein and Water for Topical Delivery of Cyclosporin A: Characterization and Study of In Vitro And In Vivo Delivery. *Eur. J. Pharm. Biopharm.* **2006**, *63*, 146−155.
(65) Qin, L.; Mei, L.; Shan, Z.; Huang, Y.; Pan, X.; Li, G.; Gu, Y.; Wu, C. Phytantriol-based Liquid Crystal Provide Sustained Release of Anticancer Drug as a Novel Embolic Agent. *Drug Dev. Ind. Pharm.* **2016**, *42*, 307−316.
(66) Lee, J.; Choi, S.-U.; Yoon, M.-K.; Choi, Y. W. Kinetic Characterization of Swelling of Liquid Crystalline Phases of Glyceryl Monooleate. *Arch. Pharmacal Res.* **2003**, *26*, 880−885.
(67) Cremonez, C. P.; Bentley, M. V. L. B.; Lara, M. G. Caracterização do Intumescimento de Sistemas Líquido-Cristalinos de Fase Lamelar de Monoleína e Água Contendo Polihexametileno-biguanida. *Rev. Cienc. Farm. Basica Apl.* **2013**, *34*, 545−553.
(68) Larsson, P.; Engqvist, H.; Biermann, J.; Werner Rönnerman, E.; Forssell-Aronsson, E.; Kovács, A.; Karlsson, P.; Helou, K.; Parris, T. Z. Optimization of Cell Viability Assays to Improve Replicability and Reproducibility of Cancer Drug Sensitivity Screens. *Sci. Rep.* **2020**, *10*, 5798.
(69) Faergemann, J.; Zehender, H.; Millerioux, L. Levels of terbinafine In Plasma, Stratum Corneum, Dermis-Epidermis (Without Stratum Corneum), Sebum, Hair and Nails During and after 250 Mg Terbinafine Orally Once Daily For 7 and 14 Days. *Clin. Exp. Dermatol.* **1994**, *19*, 121−126.
(70) Hosseini-Yeganeh, M.; McLachlan, A. J. Physiologically Based Pharmacokinetic Model for Terbinafine in Rats and Humans. *Antimicrob. Agents Chemother.* **2002**, *46*, 2219−2228.
(71) Shah, V. P.; Epstein, W. L.; Riegelman, S. Role of Sweat in Accumulation of Orally Administered Griseofulvin in Skin. *J. Clin. Invest.* **1974**, *53*, 1673−1678.
(72) Bruno, C. D.; Harmatz, J. S.; Duan, S. X.; Zhang, Q.; Chow, C. R.; Greenblatt, D. J. Effect of Lipophilicity on Drug Distribution and Elimination: Influence of Obesity. *Br. J. Clin. Pharmacol.* **2021**, *87*, 3197.
(73) Hultin, T. A.; May, C. M.; Moon, R. C. N-(4-hydroxyphenyl)-all-trans-retinamide Pharmacokinetics in Female Rats and Mice. *Drug Metab. Dispos.* **1986**, *14*, 714−717.
(74) Wood, G. W.; Neff, J. E.; Stephens, R. Relationship Between Monocytosis and T-Lymphocyte Function in Human Cancer. *J. Natl. Cancer Inst.* **1979**, *63*, 587−592.
(75) Koenig, B. W.; Gawrisch, K. Specific Volumes of Unsaturated Phosphatidylcholines in the Liquid Crystalline Lamellar Phase. *Biochim. Biophys. Acta* **2005**, *1715*, 65−70.
(76) Papahadjopoulos, D.; Watkins, J. C. Phospholipid Model Membranes. II. Permeability Properties of Hydrated Liquid Crystals. *Biochim. Biophys. Acta* **1967**, *135*, 639−652.
(77) Pakkanen, K. I.; Duelund, L.; Qvortrup, K.; Pedersen, J. S.; Ipsen, J. H. Mechanics and Dynamics of Triglyceride-Phospholipid Model Membranes: Implications for Cellular Properties And Function. *Biochim. Biophys. Acta* **2011**, *1808*, 1947−1956.
(78) Boyd, B. J.; Whittaker, D. V.; Khoo, S. M.; Davey, G. Lyotropic Liquid Crystalline Phases Formed from Glycerate Surfactants as Sustained Release Drug Delivery Systems. *Int. J. Pharm.* **2006**, *309*, 218−226.
(79) Geraghty, P. B.; Attwood, D.; Collett, J. H.; Dandiker, Y. The in Vitro Release of Some Antimuscarinic Drugs from Monoolein/Water Lyotropic Liquid Crystalline Gels. *Pharm. Res.* **1996**, *13*, 1265−1271.
(80) Dully, M.; Brasnett, C.; Djeghader, A.; Seddon, A.; Neilan, J.; Murray, D.; Butler, J.; Soulimane, T.; Hudson, S. P. Modulating the Release of Pharmaceuticals from Lipid Cubic Phases Using a Lipase Inhibitor. *J. Colloid Interface Sci.* **2020**, *573*, 176−192.
(81) Hansen, A. H.; Mouritsen, O. G.; Arouri, A. Enzymatic Action of Phospholipase A2 on Liposomal Drug Delivery Systems. *Int. J. Pharm.* **2015**, *491*, 49−57.
(82) Iwata, T.; Kobayashi, S.; Tabata, K.; Yonezawa, N.; Doi, Y. Crystal Structure, Thermal Behavior and Enzymatic Degradation of Poly (tetramethylene adipate) Solution-Grown Chain-Folded Lamellar Crystals. *Macromol. Biosci.* **2004**, *4*, 296−307.
(83) Wang, D.; Ma, B.; Wang, Z.; Zhao, Y.; Sun, Y.; Luan, Y.; Wang, J. Preparation and Characterization of B-Casein Stabilized Lipopeptide Lyotropic Liquid Crystal Nanoparticles for Delivery of Doxorubicin. *Soft Matter* **2019**, *15*, 9011−9017.
(84) Bhatt, A.; Barnes, T.; Prestidge, C. Silica Nanoparticle Stabilization of Liquid Crystalline Lipid Dispersions: Impact on Enzymatic Digestion and Drug Solubilization. *Curr. Drug Deliv.* **2015**, *12*, 47−55.
(85) Porter, C. J. H.; Pouton, C. W.; Cuine, J. F.; Charman, W. N. Enhancing Intestinal Drug Solubilisation Using Lipid-Based Delivery Systems. *Adv. Drug Deliv. Rev.* **2008**, *60*, 673−691.

https://doi.org/10.1021/acs.molpharmaceut.1c00319
Mol. Pharmaceutics 2021, 18, 3401−3417

(86) Tan, A.; Simovic, S.; Davey, A. K.; Rades, T.; Boyd, B. J.; Prestidge, C. A. Silica Nanoparticles to Control the Lipase-Mediated Digestion of Lipid-Based Oral Delivery Systems. *Mol. Pharm.* **2010**, *7*, 522−532.
(87) Spadari, C. d. C.; de Bastiani, F. W. M. d. S.; Lopes, L. B.; Ishida, K. Alginate Nanoparticles As Non-Toxic Delivery System for Miltefosine in the Treatment of Candidiasis And Cryptococcosis. *Int. J. Nanomed.* **2019**, *14*, 5187.
(88) Li, Q.-L.; Sun, Y.; Sun, Y.-L.; Wen, J.; Zhou, Y.; Bing, Q.-M.; Isaacs, L. D.; Jin, Y.; Gao, H.; Yang, Y.-W. Mesoporous Silica Nanoparticles Coated by Layer-by-Layer Self-Assembly Using Cucurbit [7] Uril for In Vitro and In Vivo Anticancer Drug Release. *Chem. Mater.* **2014**, *26*, 6418−6431.
(89) Duan, J.; Zhang, Y.; Han, S.; Chen, Y.; Li, B.; Liao, M.; Chen, W.; Deng, X.; Zhao, J.; Huang, B. Synthesis and In Vitro/In Vivo Anti-Cancer Evaluation of Curcumin-Loaded Chitosan/Poly (Butyl Cyanoacrylate) Nanoparticles. *Int. J. Pharm.* **2010**, *400*, 211−220.
(90) Shafaa, M. W. Preparation, characterization and Evaluation of Cytotoxic Activity of Tamoxifen Bound Liposomes Against Breast Cancer Cell Line. *Egypt. J. Biomed. Eng. Biophys.* **2020**, *21*, 19−31.
(91) Cheng, X.; Kuhn, L. Chemotherapy Drug Delivery from Calcium Phosphate Nanoparticles. *Int. J. Nanomed.* **2007**, *2*, 667.
(92) Lundberg, B. B.; Griffiths, G.; Hansen, H. J. Cellular Association And Cytotoxicity Of Doxorubicin-Loaded Immunoliposomes Targeted via Fab'fragments of an Anti-CD74 Antibody. *Drug Deliv.* **2007**, *14*, 171−175.
(93) Chaudhuri, S.; Fowler, M. J.; Baker, C.; Stopka, S. A.; Regan, M. S.; Sablatura, L.; Broughton, C. W.; Knight, B. E.; Stabenfeldt, S. E.; Agar, N. Y. R.; Sirianni, R. W. β-Cyclodextrin-Poly (β-Amino Ester) Nanoparticles Are a Generalizable Strategy for High Loading and Sustained Release of HDAC Inhibitors. *ACS Appl. Mater. Interfaces* **2021**, *13*, 20960−20973.
(94) de Menezes, D. E. L.; Pilarski, L. M.; Allen, T. M. In Vitro and In Vivo Targeting of Immunoliposomal Doxorubicin oo Human B-Cell Lymphoma. *Cancer Res.* **1998**, *58*, 3320−3330.
(95) Zhang, L.; Huang, D.; Shao, D.; Liu, H.; Zhou, Q.; Gui, S.; Wei, W.; Wang, Y. Fenretinide Inhibits the Proliferation and Migration of Human Liver Cancer Hepg2 Cells by Downregulating the Activation of Myosin Light Chain Kinase through the p38MAPK Signaling Pathway. *Oncol. Rep.* **2018**, *40*, 518−526.
(96) Kang, H.; Lee, M.; Choi, K.-c.; Shin, D.-M.; Ko, J.; Jang, S.-W. N-(4-hydroxyphenyl) Retinamide Inhibits Breast Cancer Cell Invasion Through Suppressing NF-KB Activation and Inhibiting Matrix Metalloproteinase-9 Expression. *J. Cell. Biochem.* **2012**, *113*, 2845−2855.
(97) Helbig, G.; Christopherson, K. W.; Bhat-Nakshatri, P.; Kumar, S.; Kishimoto, H.; Miller, K. D.; Broxmeyer, H. E.; Nakshatri, H. NF-κ B Promotes Breast Cancer Cell Migration and Metastasis by Inducing The Expression of the Chemokine Receptor CXCR4. *J. Biol. Chem.* **2003**, *278*, 21631−21638.
(98) Benelli, R.; Monteghirfo, S.; Venè, R.; Tosetti, F.; Ferrari, N. The Chemopreventive Retinoid 4HPR Impairs Prostate Cancer Cell Migration and Invasion by Interfering with FAK/AKT/GSK3β Pathway and β-Catenin Stability. *Mol. Canc.* **2010**, *9*, 142.
(99) Carvalho, V. F. M.; Migotto, A.; Giacone, D. V.; de Lemos, D. P.; Zanoni, T. B.; Maria-Engler, S. S.; Costa-Lotufo, L. V.; Lopes, L. B. Co-encapsulation of Paclitaxel And C6 Ceramide in Tributyrin-Containing Nanocarriers Improve Co-Localization in the Skin and Potentiate Cytotoxic Effects in 2D and 3D Models. *Eur. J. Pharm. Sci.* **2017**, *109*, 131−143.
(100) Mattern-Schain, S. I.; Fisher, R. K.; West, P. C.; Grimsley, L. B.; Harris, T. M.; Grandas, O. H.; Best, M. D.; Mountain, D. J. H. Cell Mimetic Liposomal Nanocarriers for Tailored Delivery of Vascular Therapeutics. *Chem. Phys. Lipids* **2019**, *218*, 149−157.
(101) Collnot, E.-M.; Baldes, C.; Wempe, M. F.; Kappl, R.; Hüttermann, J.; Hyatt, J. A.; Edgar, K. J.; Schaefer, U. F.; Lehr, C.-M. Mechanism of Inhibition of P-Glycoprotein Mediated Efflux by Vitamin E TPGS: Influence on Atpase Activity and Membrane Fluidity. *Mol. Pharm.* **2007**, *4*, 465−474.
(102) Pepe, D.; Phelps, J.; Lewis, K.; Dujack, J.; Scarlett, K.; Jahan, S.; Bonnier, E.; Milic-Pasetto, T.; Hass, M. A.; Lopes, L. B. Decylglucoside-based Microemulsions for Cutaneous Localization of Lycopene and Ascorbic Acid. *Int. J. Pharm.* **2012**, *434*, 420−428.
(103) Bernhofer, L. P.; Barkovic, S.; Appa, Y.; Martin, K. M. IL-1alpha and IL-1ra Secretion from Epidermal Equivalents and the Prediction of the Irritation Potential of Mild Soap and Surfactant-based Consumer Products. *Toxicol. In Vitro* **1999**, *13*, 231−239.
(104) Heidor, R.; Festa Ortega, J.; de Conti, A.; Prates Ong, T.; Salvador Moreno, F. Anticarcinogenic Actions of Tributyrin, a Butyric Acid Prodrug. *Curr. Drug Targets* **2012**, *13*, 1720−1729.
(105) Kang, S. N.; Hong, S. S.; Lee, M. K.; Lim, S. J. Dual Function of Tributyrin Emulsion: Solubilization and Enhancement of Anticancer Effect Of Celecoxib. *Int. J. Pharm.* **2012**, *428*, 76−81.
(106) Shin, J. H.; Shin, D. H.; Kim, J. S. Let-7 miRNA and CDK4 siRNA co-encapsulated in Herceptin-conjugated Liposome for Breast Cancer Stem Cells. *Asian J. Pharm. Sci.* **2020**, *15*, 472−481.
(107) Bassani, B.; Bartolini, D.; Pagani, A.; Principi, E.; Zollo, M.; Noonan, D. M.; Albini, A.; Bruno, A. Fenretinide (4-HPR) Targets Caspase-9, ERK 1/2 and the Wnt3a/B-Catenin Pathway in Medulloblastoma Cells and Medulloblastoma Cell Spheroids. *PLoS One* **2016**, *11*, No. e0154111.
(108) Cuperus, R.; Tytgat, G.; Leen, R.; Brites, P.; Bras, J.; Caron, H.; Van Kuilenburg, A. Pleiotropic Effects of Fenretinide in Neuroblastoma Cell Lines and Multicellular Tumor Spheroids. *Int. J. Oncol.* **2008**, *32*, 1011−1019.
(109) Cuperus, R.; van Kuilenburg, A. B. P.; Leen, R.; Bras, J.; Caron, H. N.; Tytgat, G. A. M. Promising Effects of the 4HPR−BSO Combination in Neuroblastoma Monolayers and Spheroids. *Free Radical Biol. Med.* **2011**, *51*, 1213−1220.
(110) Cazzaniga, M.; Varricchio, C.; Montefrancesco, C.; Feroce, I.; Guerrieri-Gonzaga, A. Fenretinide (4-HPR): a Preventive Chance for Women at Genetic and Familial Risk? *J. Biomed. Biotechnol.* **2012**, *2012*, 172897.
(111) Brisson, B. K.; Mauldin, E. A.; Lei, W.; Vogel, L. K.; Power, A. M.; Lo, A.; Dopkin, D.; Khanna, C.; Wells, R. G.; Puré, E.; Volk, S. W. Type III Collagen Directs Stromal Organization and Limits Metastasis In a Murine Model of Breast Cancer. *Am. J. Pathol.* **2015**, *185*, 1471−1486.
(112) Lookingbill, D. P.; Spangler, N.; Helm, K. F. Cutaneous Metastases in Patients with Metastatic Carcinoma: a Retrospective Study of 4020 Patients. *J. Am. Acad. Dermatol.* **1993**, *29*, 228−236.
(113) Krathen, R. A.; Orengo, I. F.; Rosen, T. Cutaneous Metastasis: a Meta-analysis of Data. *South. Med. J.* **2003**, *96*, 164−167.
(114) Ulukaya, E.; Kurt, A.; Wood, E. J. 4-(N-hydroxyphenyl)-retinamide Can Selectively Induce Apoptosis in Human Epidermoid Carcinoma Cells but not in Normal Dermal Fibroblasts. *Canc. Invest.* **2001**, *19*, 145−154.
(115) Rodríguez-Burford, C.; Steele, V. E.; Anderson, A. S.; Stockard, C. R.; Weiss, H. L.; Eto, I.; Johanning, G. L.; Grizzle, W. E.; Grubbs, C. J. Effects of Body Weight Gain Reduction Resulting from Chemopreventive Agent Treatment on Mammary Gland Morphology. *Nutr. Canc.* **2002**, *43*, 67−75.
(116) Fleming, A. B.; Saltzman, W. M. Pharmacokinetics of the Carmustine Implant. *Clin. Pharmacokinet.* **2002**, *41*, 403−419.

https://doi.org/10.1021/acs.molpharmaceut.1c00319
Mol. Pharmaceutics 2021, 18, 3401−3417